Adaptive Output-Feedback Control with Closed-Loop Reference Models and Applications to Very Flexible Aircraft

Zheng Qu* and Anuradha Annaswamy†
Massachusetts Institute of Technology, Cambridge, MA 02139, USA.

This paper proposes an adaptive controller for a class of multi-input multi-output (MIMO) plants where the number of outputs is larger than the number of inputs, an example of which is very-flexible aircraft (VFA). A dominant presence of model uncertainties and actuator anomalies necessitates an adaptive approach for control of VFA. The proposed controller, denoted as the adaptive SPR/LTR controller, combines a baseline observer-based design with loop transfer recovery (LTR) properties and an adaptive design based on strictly positive real (SPR) transfer functions. In addition to accommodating the absence of full state measurements, the controller includes a reference model that also plays the role of an observer through a closed-loop component. Conditions are delineated under which this controller, can guarantee asymptotic reference tracking, and the control design is validated using a VFA model around a single equilibrium flight condition with 707 states, 12 outputs and 2 control inputs. Simulation results show that the adaptive controller not only ensures stability but also recovers a nominal performance both in time domain and in frequency domain despite the presence of varying wing shape and actuator anomalies.

Nomenclature

A	= Nominal state matrix with augmented errors	q	= pitch rate, rad/s
A_m	= Reference model state matrix	R	= Positive definite weight matrix
A_z	= Vertical acceleration	S_1	= Output mixing matrix
B	= Nominal input matrix	t	= Time, sec
B_z	= Nominal reference input matrix	u	= Control input
C	= Nominal measured output matrix	$V(\cdot)$	= Lyapunov function candidate
C_z	= Nominal tracking output measurement matrix	V_z	= Vertical climb rate
D_z	= Nominal tracking output input matrix	x	= Plant model state
e_x	= State error	x_m	= Reference model state
e_y	= Measured output error	y	= Measured output of plant
e_z	= Tracking output error	y_m	= Reference model output
$G(s)$	= Transfer function matrix	z	= Tracking output of plant
I	= Identity matrix	z_m	= Tracking output of reference model
K	= State feedback gain	z_{cmd}	= Command of tracking output
L	= Nominal observer feedback gain	α	= Angle of attack, rad
L_v	= Observer feedback gain designed by OBLTR	Γ	= Adaptation gain
L_ρ	= Observer feedback gain designed by SPR/LTR	δ_e	= Elevator angle, rad
M	= Right null space of C	Θ^*	= Uncertainty matrix
m	= Number of input	Θ	= Adjustable parameter
N	= Left null space of B	Θ^*_{max}	= Upbound of uncertainty
n	= Number of state	Λ^*	= Uncertainty matrix
P	= Positive definite matrix for KYP Lemma	Λ	= Adjustable parameter
p	= Number of output	Λ^*_{max}	= Upbound of uncertainty
Q	= Positive definite weight matrix	η	= Dihedral angle of wing

*Ph.D Candidate, Department of Mechanical Engineering, Room 3-441.
†Senior Research Scientist, Department of Mechanical Engineering, Room 3-339A.

I. Introduction

Very Flexible Aircraft (VFA) platforms are being investigated with increased attention in the last decade, motivated to a large extent by the desire to generate high-altitude low-endurance (HALE) flights [1–3]. VFA corresponds to an aerial platform whose equilibrium flight condition (*trim*) critically depends on the flexible modes of wings [2,4]. One of the challenges of VFA is a significant change in the rigid-body dynamics around a trim as the wing morphs. For example, the pitch (short period) mode of VFA can become unstable when wing dihedral is trimmed at a high value [4,5]. As a consequence, control designs based on rigid-body dynamics only may face unexpected adversities. An example of this adversity occurred in 2003 during the second test flight of Helios when the flight controller failed to regulate the wing dihedral and eventually, allowed the unstable pitch mode to diverge [5]. The lesson learned from the mishap is that the model for control designs has to include body flexible effects [4,5].

Recently, a VFA platform, denoted as Vulture, has been under development to meet the goals of HALE maneuvers and will be used to demonstrate improved control designs [6]. Vulture is an experimental aircraft with a huge wingspan of 400ft. The entire wing is made of light low-yield material and is flexible to deform. A large 707-state model has been derived around a trim point, with a large number of body flexible modes [6]. A particular challenge is that only a set of state measurements can be used for control because none of the body flexible modes are measurable. The restriction necessitates control designs based on output-feedback, such as linear quadratic gaussian (LQG) controllers.

LQG controllers have been widely employed for the control of commercial aircraft and their performance is quite satisfactory for a nominal plant model [7,8]. The corresponding design procedure is to trim aircraft around an equilibrium, obtain a linearized model and design the LQG controllers so as to realize trajectory tracking near the trim. Combined with full-state LTR techniques [9,10], the resulting controllers, denoted as LQG/LTR, recover the guaranteed stability margins of linear quadratic regulators (LQR) asymptotically [9–11], and therefore can tolerate a certain amount of model uncertainties. Application of LQG/LTR controllers on VFA, however, faces unique difficulties. First, since flexible wings can deform to an unknown shape, the actual trim and the corresponding flight dynamics can drift far away from the control model (*trim drift*). Second, a HALE flight can cause severe actuator anomalies such as power surge in motors or structure damage in control surfaces. Both unknown adversities can exceed stability margins of LQG/LTR controllers, and therefore make these controllers inadequate for VFA.

The above limitations of LQG controllers motivate an adaptive control solution that is able to accommodate the unknowns associated with VFA flights. In particular, trim drift can cause the displacement of wing flexible components, which in turn changes the orientation of control surfaces in airflow, producing a state-dependent control perturbation. When actuator anomalies occur, the actual lift/thrust force can be scaled by an unknown factor, producing a multiplicative control perturbation. It can be shown that both types of the adversities can be modeled as parametric uncertainties in the underlying plant model.

In this paper, we develop an adaptive output-feedback controller that can accommodate parametric uncertainties in a typical MIMO plant model, and apply the control design on VFA models to achieve trajectory tracking despite the presence of body flexible effects. The classical approach to MIMO adaptive controllers (see Ref. [12] Chapter 10 and Ref. [13] Chapter 9) is based on pre-conditioning plant transfer function matrix. Such a design typically requires the knowledge of plant's Hermite form [14,15] and uses a non-minimal observer along with a reference model. In contrast to the classical method, the approach used in this paper is similar to Ref. [16] Chapter 14, which uses a minimal observer to generate the underlying state estimates. The state estimates are then used for both feedback (similar to LQG controllers) and parameter adaptation. In contrast to the classical approach, the same minimal observer is also used to serve as a reference model, given rise to the notion of a closed-loop reference model (CRM) recently shown to be a highly promising direction in adaptive control [17–19]. The resulting adaptive output-feedback controller needs much fewer integrators than the classical controllers, and guarantees global stability and asymptotic tracking by utilizing SPR properties of an underlying transfer function. In addition, the full-state LTR properties of LQG/LTR controllers are retained in the baseline design. We denote the proposed controller as adaptive SPR/LTR controllers. The preliminary results of this paper has been presented in Ref. [20] and Ref. [21]. An alternate approach of the observer parameter design using linear matrix inequality techniques was developed in Ref. [22].

The paper is organized as follows. Section II introduces mathematical preliminaries necessary for the design and analysis of the proposed controller. Section III formulates the control problem in the context of VFA. Section IV presents the adaptive controller design and its SPR/LTR properties, and also includes stability analysis of the adaptive system. Section V demonstrates the response of the resulting closed-loop system with the adaptive controller using two numerical examples, including a simplified 3-wing VFA model and a linear model of Vulture VFA [6] around a single flight condition.

II. Preliminaries

A few definitions and lemmas are presented in this section. Proofs of all lemmas in this section are redirected to the corresponding references.

Definition 1. *The notation $\{A, B, C, D\}$ is defined as the transfer function matrix $C(sI - A)^{-1}B + D$.*

The case when $D = 0$ is denoted as $\{A, B, C\}$. We define transmission zeros in the following.

Definition 2. [23] *For a non-degenerate linear system with minimal realization $A \in \mathbb{R}^{n\times n}$, $B \in \mathbb{R}^{n\times m}$, $C \in \mathbb{R}^{p\times n}$ and $D \in \mathbb{R}^{p\times m}$, the transmission zeros are defined as the finite values of s such that rank$[R(s)] < \min(n + m, n + p)$, where*

$$R(s) = \begin{bmatrix} sI - A & B \\ C & D \end{bmatrix}. \tag{1}$$

Most non-square systems don't have transmission zeros; square systems are more likely to lose rank and therefore more likely to have transmission zeros[24]. With the definition of transmission zeros, the definition of minimum phase systems becomes a natural extension from that of SISO systems.

Definition 3. *The system is minimum phase if all transmission zeros are in open left half of the complex plane $\mathbb{C}^-$.*

It is clear that a minimum phase MIMO system does not require zeros of each individual transfer functions to be stable. One special category of minimum phase systems is a strictly positive real (SPR) system (or transfer function matrix). This paper uses Ref.[12] (see Definition 2.10) for the definition of SPR. Kalman–Yakubovich–Popov (KYP) lemma links the frequency domain properties of an SPR transfer function to its realization.

Lemma 1. *[KYP Lemma] A system $\{A, B, C\}$ is strictly positive real if and only if there exists a $P = P^T > 0$ such that*

$$PA + A^T P < 0 \tag{2}$$
$$PB = C^T. \tag{3}$$

An SPR transfer function is a square system satisfying $CB = B^T PB = (CB)^T > 0$. This paper considers square systems whose CB is full rank. Such systems have the following property.

Lemma 2. [25] *Given a pair $C \in \mathbb{R}^{m\times n}$ and $B \in \mathbb{R}^{n\times m}$, if CB has full rank, there exist matrices $M \in \mathbb{R}^{n\times(n-m)}$ and $N \in \mathbb{R}^{(n-m)\times n}$ such that $NB = 0_{(n-m)\times m}$, $CM = 0_{m\times(n-m)}$ and $NM = I_{(n-m)\times(n-m)}$.*

In this context, N is called the null space of B and M is called the null space of C. With the definition of N, Eq.(3) of KYP Lemma can be fully characterized as following.

Lemma 3. [26] *Given a pair of C and B, if there exists a $P = P^T > 0$ such that $PB = C^T$, then $P \in \mathscr{P}$ where*

$$\mathscr{P} = \{P > 0 \mid P = C^T(CB)^{-1}C + N^T W_p N, \quad W_p > 0\} \tag{4}$$

where N is the right null space of B and W_p is an arbitrary symmetric positive definite (SPD) matrix.

Proofs of Lemmas 2 and 3 can be found Ref.[25] and Ref.[26], respectively. Lemma 3 implies that there is a one-to-one correspondence between W_p and P that satisfies (4). We present another property of CB-full-rank square systems in Lemma 4 whose proof can be found in Ref.[23].

Lemma 4. [23] *For a square system $\{A, B, C\}$ with CB being full rank, the square matrix (NAM) is the zero dynamics of the system with its eigenvalue being the transmission zeros.*

From Lemma 4, it can be concluded that the minimum-phase property in Definition 3 is a necessary condition for the system to be SPR. This can be shown by pre and post-multiplying Eq.(2) with M^T and M , respectively, and appealing Eq.(4) yields

$$W_p NAM + M^T A^T N^T W_p < 0. \tag{5}$$

For Eq.(5) to hold for an SPD W_p, NAM has to be Hurwitz.

III. Problem Statement

Aircraft dynamics around an equilibrium flight condition can be represented by a linear time invariant (LTI) model as

$$\begin{aligned} \dot{x}_p &= A_p x_p + B_p u \\ y_p &= C_p x_p \\ z &= C_{pz} x_p + D_{pz} u \end{aligned} \tag{6}$$

where $x_p \in \mathbb{R}^{n_p}$ are states, $u \in \mathbb{R}^m$ are control input, $y_p \in \mathbb{R}^{p_p}$ are measurement outputs and $z \in \mathbb{R}^r$ are tracking outputs. Since in most flight control applications, there are more sensors than actuators, and all states are not measurable, we assume that $n_p > p_p \geq m$. The matrices have dimensions $A_p \in \mathbb{R}^{n_p \times n_p}$, $B_p \in \mathbb{R}^{n_p \times m}$, $C_p \in \mathbb{R}^{p_p \times n_p}$, $C_{pz} \in \mathbb{R}^{r \times n_p}$ and $D_{pz} \in \mathbb{R}^{r \times m}$ and are assumed to be known. Since z typically includes non-strictly proper outputs such as accelerations, a constant matrix D_{pz} is assumed to be present. When y_p includes non-strictly proper outputs, they are integrated to become strictly proper outputs.

Eq.(6) corresponds to the ideal case where all plant matrices are known. In reality, these matrices are unknown and are identified through various methods. The state matrix A_p can be determined through wind-tunnel tests fairly accurately. C_p and C_{pz} are well known as well since the relation between measured outputs and states is well defined. The input matrix B_p and D_{pz}, in contrast, may not be accurate as control inputs are subjected to perturbations in a VFA flight. We address two of the dominant issues in this paper.

The first source of control perturbations we consider is the orientation change of control surfaces when the flexible wing shape settles down to a value different from the trim as represented by the nominal model. In such a case, the vertical lift produced on control surfaces may be increased or reduced. This effect can be modeled as an additive term $\Theta^{*T}\Phi(x_p)$ where $\Phi(\cdot) : \mathbb{R}^{n_p} \to \mathbb{R}^d$ is a known nonlinear function which maps the flexible positions of VFA (which are part of states x_p) to each local wing dihedral. $\Theta^* \in \mathbb{R}^{d \times m}$ represents the map from a local wing dihedral to the lift adjustment of each control surface and in general is unknown.

The second source of control perturbation that we address is actuator anomalies caused by electronic power surge or control surface damage. This is modeled as an unknown multiplicative factor $\Lambda^* \in \mathbb{R}^{m \times m}$. Together, both uncertainties lead to a modified plant model given by

$$\begin{aligned} \dot{x}_p &= A_p x_p + B_p \Lambda^* [u + \Theta^{*T} \Phi(x_p)] \\ y_p &= C_p x_p \\ z &= C_{pz} x_p + D_{pz} \Lambda^* [u + \Theta^{*T} \Phi(x_p)] \end{aligned} \tag{7}$$

which is the plant model considered in Ref.[16] (Chapter 14). The uncertainties in (7) are parametric and are given by Λ^* and Θ^*. The underlying control problem is to design $u(t)$ such that in the presence of the uncertainties, $z(t)$ follows a specified reference $z_m(t)$, i.e. *reference tracking*.

The adaptive controller that we will present requires the following assumptions regarding the plant model in (7):

Assumption 1. (A_p, B_p) is controllable and (A_p, C_p) is observable;

Assumption 2. $\{A_p, B_p, C_p\}$ is minimum phase;

Assumption 3. $\{A_p, B_p, C_{pz}, D_{pz}\}$ does not have a transmission zero at the origin;

Assumption 4. $rank(C_p B_p) = m$.

Assumption 5. Λ^* is diagonal, full rank, bounded by a known value, $\|\Lambda^*\| < \Lambda^*_{max}$ and the sign of each element $sign(\Lambda^*)$ is known;

Assumption 6. Θ^* is bounded by a known value, $\|\Theta^*\| < \Theta^*_{max}$; $\Phi(\cdot)$ is globally differentiable, and is globally Lipschitz continuous, i.e. there exists a finite constant $l_\phi \in \mathbb{R}$ such that $\forall x_1, x_2 \in \mathbb{R}^{n_p}$,

$$\|\Phi(x_1) - \Phi(x_2)\| \leq l_\phi \|x_1 - x_2\|. \tag{8}$$

Assumption 1 is standard. The fact that the underlying plant model is non-square and typically has no transmission zeros[24] makes Assumption 2 reasonable. Assumption 3 usually holds, especially when $D_{pz} \neq 0$.

For nominal MIMO plant models satisfying Assumptions 1 to 3, a baseline observer-based controller (such as LQG/LTR[9]) can be designed to achieve a satisfactory tracking performance with adequate stability margins. Assumptions 4 to 6 are needed for the proposed adaptive controller. Of these, Assumption 4 is perhaps the most restrictive one, and can be viewed as the MIMO counterpart of a relative degree one assumption (see Ref.[12] Chapter 5). Assumption 5 implies that the actuator anomalies are bounded and independent from each other, and are bounded. Assumption 6 is commonly satisfied for the aerial platforms with varying dihedral wingshape, such as VFA.

IV. Adaptive SPR/LTR Controller

This section presents the adaptive output-feedback controller. Section A first introduces the architecture of the controller, which includes an observer that also doubles as a CRM. The adaptation law is also shown in this section. Section B presents the design of observer parameters and their SPR and LTR properties, as well as stability analysis of the adaptive system. Section C summarizes the overall design procedure, and Section D compares our design with other adaptive output-feedback controllers recently proposed[16,21,22]. The main challenge in our controller design is in the selection of the observer parameters so as to ensure that an underlying transfer function matrix is SPR. This is carried out in Section B, and described in Lemmas 8 and Theorem 1.

A. Controller Structure

Following the design procedure in Ref.[16] (see Chapter 14), the controller is divided into two parts, a baseline observer-based controller with an integral error modification, and an adaptive component augmentation.

1. Addition of Integral Error

Suppose a piecewise continuous command $z_{cmd}(t)$ is prescribed. For the purpose of command tracking, we first introduce an integral error state $e_{pz} = z - z_{cmd}$ and $w_{pz} := \int e_{pz} dt$, which leads to a modified plant model:

$$\begin{aligned}
\begin{bmatrix} \dot{x}_p \\ \dot{w}_{pz} \end{bmatrix} &= \underbrace{\begin{bmatrix} A_p & 0 \\ C_{pz} & 0 \end{bmatrix}}_{A} \underbrace{\begin{bmatrix} x_p \\ w_{pz} \end{bmatrix}}_{x} + \underbrace{\begin{bmatrix} B_p \\ D_{pz} \end{bmatrix}}_{B} \Lambda^* [u + \Theta^{*T} \Phi(x_p)] + \underbrace{\begin{bmatrix} 0 \\ -I \end{bmatrix}}_{B_z} z_{cmd} \\
y &= \underbrace{\begin{bmatrix} C_p & 0 \\ 0 & I \end{bmatrix}}_{C} x \\
z &= \underbrace{\begin{bmatrix} C_{pz} & 0 \end{bmatrix}}_{C_z} x + \underbrace{\begin{bmatrix} D_{pz} \end{bmatrix}}_{D_z} \Lambda^* [u + \Theta^{*T} \Phi(x_p)].
\end{aligned} \tag{9}$$

Eq.(9) can be written compactly as (10):

$$\begin{aligned}
\dot{x} &= Ax + B\Lambda^* [u + \Theta^{*T} \Phi(x_p)] + B_z z_{cmd} \\
y &= Cx \\
z &= C_z x + D_z \Lambda^* [u + \Theta^{*T} \Phi(x_p)].
\end{aligned} \tag{10}$$

Define $n := n_p + r$ and $p := p_p + r$. Then $x \in \mathbb{R}^n$ and $y \in \mathbb{R}^p$. We note that (A, B) is controllable because of Assumptions 1 and 3, and (A, C) is observable because Assumption 1 holds and the additional error states are also measured. Moreover, $rank(CB) = m$ since Assumption 4 holds.

2. Augmentation Architecture

We choose the control input u in (10) as

$$u = u_{bl} + u_{ad} \tag{11}$$

where u_{bl} is determined using a baseline observer-based controller and u_{ad} by an adaptive controller. The baseline control u_{bl} is chosen as

$$u_{bl} = -Kx_m \tag{12}$$

where K is designed by applying the linear quadratic regulator (LQR) technique on the nominal plant model $\{A, B, C\}$, and x_m is the output of the state observer

$$\begin{aligned} \dot{x}_m &= Ax_m + Bu_{bl} + B_z z_{cmd} + L_\rho(y - y_m) \\ y_m &= Cx_m \\ z_m &= C_z x_m + D_z u_{bl}. \end{aligned} \tag{13}$$

which also serves as a CRM [17–19]. One can see the form of a CRM in (13) by substituting u_{bl} with Eq.(12). Eq.(13) serves two purposes, one of an observer, where L_ρ is equivalent to an observer gain, whose purpose is to provide a state estimate, and the other of a reference model, whose purpose is to provide a reference for the states. While L_ρ can be chosen using the LTR techniques when the uncertainties Λ^* and Θ^* are zero, its design in the presence of uncertainties will depend also on an underlying SPR transfer function, which will be discussed in greater detail in Section 1 and 2.

The adaptive component u_{ad} is chosen as

$$u_{ad} = -[I - \Lambda^{-1}(t)]u_{bl} - \Theta^T(t)\Phi(x_{mp}) \tag{14}$$

where x_{mp} is the first n_p elements of x_m, corresponding to the estimate of x_p. It is noted that the inverse sign in $\Lambda^{-1}(t)$ is for notation purpose only, i.e. $\Lambda(t)$ does not necessarily exists. $\Lambda^{-1}(t)$ and $\Theta^T(t)$ are estimates of Λ^{*-1} and Θ^{*T}, respectively, both of which are to be suitably adjusted. To determine their adjustment, we derive the error model for $e_x = x - x_m$ by subtracting (13) from (10) as

$$\begin{aligned} \dot{e}_x &= Ax + Bu_{bl} + B_z z_{cmd} + B\Lambda^*[u_{ad} + (I - \Lambda^{*-1})u_{bl} + \Theta^{*T}\Phi(x_p)] \\ &\quad -Ax_m - Bu_{bl} - B_z z_{cmd} - L_\rho(y - y_m) \\ &= (A - L_\rho C)e_x + \mathfrak{U}(x_p, x_{mp}) + B\Lambda^*[\widetilde{\Lambda}^T u_{bl} - \widetilde{\Theta}^T\Phi(x_{mp})] \end{aligned} \tag{15}$$

where $\mathfrak{U}(x_p, x_{mp}) := B\Lambda^*\Theta^{*T}[\Phi(x_p) - \Phi(x_{mp})]$, $\widetilde{\Lambda}^T(t) := \Lambda^{-1}(t) - \Lambda^{*-1}$, and $\widetilde{\Theta}^T(t) := \Theta^T(t) - \Theta^{*T}$. The structure of (15) suggests the following adaptive laws (see also Ref. [16])

$$\begin{aligned} \dot{\Theta}(t) &= \Gamma_\theta \Phi(x_{mp}) e_y^T S_1^T sign(\Lambda^*) \\ \dot{\Lambda}^{-T}(t) &= -\Gamma_\lambda u_{bl} e_y^T S_1^T sign(\Lambda^*) \end{aligned} \tag{16}$$

where $\Gamma_\theta > 0, \Gamma_\lambda > 0$ are update gains, $e_y = y - y_m$ and $S_1 \in \mathbb{R}^{m \times p}$ is an output-mixing matrix which will be designed together with L_ρ in Section 1. The novelty in adaptation law (16) is that the state estimate $x_m(t)$ and the output errors e_y are used, which enables us to perform output feedback adaptation. Under the SPR conditions on an underlying transfer function matrix and with Assumptions 5 and 6, it can be shown that the adaptive controller given by (11)(12)(13)(14) and (16) (shown in Figure 1) leads to global asymptotic stability and reference tracking. This is addressed in detail in Section B, along with the design of L_ρ and S_1.

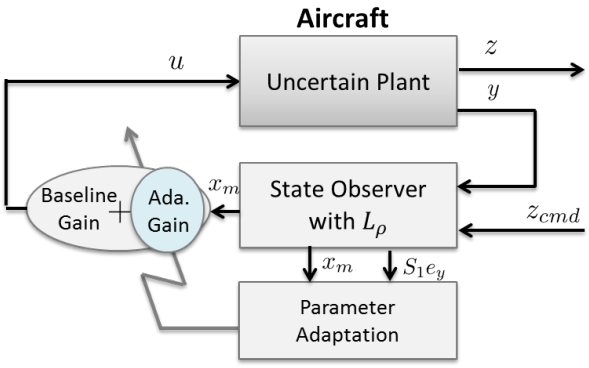

Figure 1. The architecture of the adaptive SPR/LTR controller: the adaptive component is added to a baseline observer-based controller

B. SPR/LTR Design

L_ρ in the observer/CRM (13) and S_1 in the adaptation law (16) will be chosen such that an underlying transfer function matrix is SPR. Section 1 presents the SPR design for a simpler case when $\Theta^* = 0$ in (10), and Section 2 addresses the general case when $\Theta^* \neq 0$. The SPR design for both cases as well as the stability analysis of the adaptive system is presented in these sections as well. The LTR properties of L_ρ in the baseline controller are introduced in Section 3. All proofs can be found in the Appendix.

1. Nominal SPR Design: $\Theta^* = 0$

Since $\Theta^* = 0$, we choose $\Theta(t) \equiv 0$ and denote L_ρ as L. The only uncertainty existing in the plant model (10) is Λ^*. Lemma 5 guarantees stability of the adaptive design under the SPR conditions of $\{(A - LC), B, S_1C\}$. Define $e_x = x - x_m$.

Lemma 5. *For the uncertain plant model (10) with $\Theta^* = 0$, satisfying Assumptions 1 to 5, if a pair of L and S_1 are chosen such that $\{(A - LC), B, S_1C\}$ is SPR, the adaptive SPR/LTR controller (11)(12)(13)(14)(16) with $L = L_\rho$ and $\Theta(t) \equiv 0$, guarantees that i) the closed-loop system has bounded solutions and ii) $e_x(t) \to 0$ as $t \to \infty$.*

Since $\widetilde{\Theta} = 0$ and $L_\rho = L$, the error model (15) becomes

$$\dot{e}_x = (A - LC)e_x + B\Lambda^*\widetilde{\Lambda}^T u_{bl}. \tag{17}$$

Eq.(17) reveals that the underlying transfer function matrix $\{(A - LC), B, S_1C\}$ represents the signal path from $\widetilde{\Lambda}^T u_{bl}$ to $S_1 e_y$. The conditions of Lemma 5 imply that this signal path is SPR, meaning that $\widetilde{\Lambda}^T u_{bl}$ and $S_1 e_y$ is always in the same direction[27]. The directionality is utilized in the adaptation law (16) to adjust parameters suitably.

The matrices L and S_1 that make the required signal path SPR are referred to as "SPR pairs" and are to be determined. Using Lemma 1 (KYP Lemma), the design goal can be transformed into: given $\{A, B, C\}$, find an SPR pair such that there exists a $Q > 0$ that can produce a solution $P = P^T > 0$ to the following equations:

$$(A - LC)^T P + P(A - LC) = -Q < 0 \tag{18}$$

$$PB = C^T S_1^T. \tag{19}$$

The design in (18)(19) is the "feedback SPR designs" that have been attempted previously[21,22,26,28]. In contrast to the designs in Ref.[26,28] that requires $CB > 0$, the method in this paper extends the results to non-square plant models with CB being full rank. Comparison between our method and Ref.[21,22] is discussed in detail in Section D. We now describe how an SPR pair can be designed.

First, a $\bar{B}$ is designed by appending B with a $B_2 \in \mathbb{R}^{n\times(p-m)}$, i.e.

$$\bar{B} = [B, B_2] \tag{20}$$

where B_2 represents the pseudo-inputs that are designed to square-up the system $\{A, \bar{B}, C\}$, keep it minimum phase and also satisfy that $C\bar{B}$ is full rank. Under Assumptions 1 to 4, B_2 can be designed using the method in Ref.[29] for a plant model without transmission zeros, or using the modified method in Ref.[30] for a plant model with minimum-phase transmission zeros. An output-mixing matrix S and $\bar{C}$ are designed as

$$S := [S_1, S_2] = (C\bar{B})^T \tag{21}$$

$$\bar{C} := SC. \tag{22}$$

$S_1 \in \mathbb{R}^{m\times p}$ is a sub-matrix of S. A $\mu^* \in \mathbb{R}$ is chosen such that

$$0 < \mu^* < |\mu_{max}| \tag{23}$$

where μ_{max} is the maximum real part of the transmission zeros of $\{A, \bar{B}, \bar{C}\}$. An $\bar{A}$ is designed as

$$\bar{A} = A + \mu^* I. \tag{24}$$

A finite L is calculated as

$$L = \bar{B}R^{-1}S \tag{25}$$

where R^{-1} is designed by applying the output-feedback SPR method[28] on $\{\bar{A}, \bar{B}, \bar{C}\}$:

$$R^{-1} = (\bar{C}\bar{B})^{-1}((\bar{C}\bar{A}\bar{B})^T + \bar{C}\bar{A}\bar{B})(\bar{C}\bar{B})^{-1} + \epsilon I > 0 \ . \tag{26}$$

The finite constant ϵ in (26) should be chosen to be large enough such that

$$\begin{gathered} \epsilon > \epsilon^*, \quad \epsilon^* = \max\left[\epsilon_1^*, \epsilon_2^*\right] \\ \epsilon_1^* = \lambda_{max}\left\{-(\bar{C}\bar{B})^{-1}((\bar{C}\bar{A}\bar{B})^T + \bar{C}\bar{A}\bar{B})(\bar{C}\bar{B})^{-1}\right\} \\ \epsilon_2^* = \lambda_{max}\left\{(\bar{C}\bar{B})^{-1}H^T Q_I^{-1} H(\bar{C}\bar{B})^{-1}\right\} \end{gathered} \tag{27}$$

where $\lambda_{max}(\cdot)$ stands for the maximum real part of the eigenvalues and

$$H := M^T\bar{A}^T\bar{C}^T + P_I N\bar{A}\bar{B}. \tag{28}$$

N is the null space of $\bar{B}$ and M is the null space of $\bar{C}$ satisfying $NM = I$ (see Lemma 2). P_I is the unique solution to a Lyapunov equation

$$P_I N\bar{A}M + M^T\bar{A}^T N^T P_I = -Q_I. \tag{29}$$

Once a $Q_I > 0$ is chosen, a finite $P_I > 0$ can always be found since $N\bar{A}M$ is the zero dynamics of $\{\bar{A}, \bar{B}, \bar{C}\}$ and hence is Hurwitz. It is noted that Q_I scales P_I. Different from Ref.[28], we choose a $Q_I > 0$ such that

$$P_I \geq \lambda_{max}\left\{M^T[I + \bar{B}^T(\bar{C}\bar{B})^{-1}\bar{B}^T]M\right\} I_{(n-m)}. \tag{30}$$

Eq.(20) to Eq.(30) complete our design of L and S_1. It is noted that the pseudo-input matrix B_2 is only used to design L and not used as real control inputs. Intuitively, L transforms LC into an output-feedback direction $\bar{B}R^{-1}\bar{C}$, , which, if large enough, overwhelms the error state dynamics in (17) and aligns the directions of $\widetilde{\Lambda}^T u_{bl}$ and $S_1 e_y$. This is formally summarized in Lemma 6.

Lemma 6. *Given a MIMO plant model $\{A, B, C\}$ that satisfies Assumptions 2 to 4, the finite pair of $L \in \mathbb{R}^{n\times p}$ as in (25) and $S_1 \in \mathbb{R}^{m\times p}$ as in (21) guarantees that $\forall\mu \in \mathbb{R}$ satisfying $0 \leq \mu \leq \mu^*$, the transfer function matrix $\{(A + \mu I - LC), B, S_1 C\}$ is strictly positive real.*

Lemma 6 extends the results in Ref.[28] to a non-square plant model with a class of $(A + \mu I)$. Lemma 6 (choosing $\mu = 0$) and Lemma 5 complete the controller design for the $\Theta^* = 0$ case.

2. Robust SPR Design: $\Theta^* \neq 0$

When $\Theta^* \neq 0$, the L_ρ design in CRM (13) depends on the bound of Ψ^*, where Ψ^* is defined as

$$\Psi^* := \frac{l_\phi^2}{4}\Lambda^*\Theta^{*T}\Theta^*\Lambda^{*T}S_1 C. \tag{31}$$

l_ϕ is defined as in (8), and S_1 is defined in (21). From Assumptions 5 and 6, a bound of Ψ^* can be calculated as

$$\|\Psi^*\| \leq \frac{l_\phi^2}{4}\Lambda_{max}^{*2}\Theta_{max}^{*2}\|S_1 C\| = \Psi_{max}^*. \tag{32}$$

Ψ_{max}^* is finite and known. We introduce the following Lemma on the stability of the adaptive system, which provides the guidelines for the design of L_ρ.

Lemma 7. *For the uncertain plant model (10) satisfying Assumptions 1 to 6, if a pair of L_ρ and S_1 are chosen such that the uncertain transfer function $\{(A + \eta I + \frac{1}{\eta}B\Psi^* - L_\rho C), B, S_1 C\}$ is guaranteed to be SPR for some $\eta > 0$, the adaptive SPR/LTR controller (11)(12)(13)(14)(16) guarantees that i) the closed-loop system has bounded solutions and ii) $e_x(t) \to 0$ as $t \to \infty$.*

The error model for the general case $\Theta^* \neq 0$ has been presented in (15). Conditions of Lemma 7 imply that the underlying directionality between $\widetilde{\Lambda}^T u_{bl}$ (or $\widetilde{\Theta}^T\Phi(x_{mp})$) and $S_1 e_y$ can still be utilized to adjust the adaptive parameters. The directionality, however, becomes implicit because of the presence of the nonlinear term $\mathfrak{U}(x_p, x_{mp})$ (see (15)). Previous adaptive output-feedback control designs[21] use the directionality implicitly in proving the stability. Lemma

7 in this paper reveals the underlying directionality explicitly, and synthesizes observer parameter designs with stability analysis, which is the central idea of our method. Lemma 5 is a special case of Lemma 7 when $\Psi^* = 0$. The case when $\Phi(x_p) = x_p$ (as considered in Ref.[21,22]), can be treated as a special case of Lemma 7 with $\Psi^* = \Lambda^*\Theta^*$ where Θ^* should be augmented with additional r columns of zeros.

We now present the design of an SPR pair for the case when $\Theta^* \neq 0$. First, we use Eq.(25) and Eq.(21) to design an SPR pair of L and S_1. Then we introduce an additional term to L as

$$L_\rho = L + \rho\bar{B}S = \bar{B}(R^{-1} + \rho I)S \tag{33}$$

where ρ is a design parameter that is chosen to be sufficiently large:

$$\rho > \rho^*, \quad \rho^* = \frac{\Psi_{max}^{*2}\|S_1\|^2}{2\mu^{*2}\lambda_{min}(\widetilde{Q})\lambda_{min}(S^TS)}. \tag{34}$$

μ^* is chosen in (23), and $\widetilde{Q}$ is found using

$$\widetilde{Q} = -N^TH(\bar{C}\bar{B})^{-1}\bar{C} - \bar{C}^T(\bar{C}\bar{B})^{-1}H^TN + \bar{C}^T(R^{-1} + \epsilon I)\bar{C} + N^TQ_IN. \tag{35}$$

It is noted that ϵ and ρ has the same effect on L_ρ, and L_ρ depends on Ψ_{max}^* instead of Ψ^*. In general, μ^* in (34) can be chosen to be any scalars smaller than μ^*. Lemma 8 validates the SPR design.

Lemma 8. *Given an uncertain plant model (10) that satisfies Assumptions 1 to 6, the finite pair of $L_\rho \in \mathbb{R}^{n\times p}$ as in (33) and $S_1 \in \mathbb{R}^{m\times p}$ as in (21) guarantees that $\forall\mu \in \mathbb{R}$ satisfying $0 \leq \mu \leq \mu^*$ and $\forall\Psi \in \mathbb{R}^{m\times n}$ bounded by $\|\Psi\| \leq \Psi_{max}^*$, the uncertain transfer function matrix $\{(A + \mu I + \frac{1}{\mu^*}B\Psi - L_\rho C), B, S_1C\}$ is strictly positive real.*

With Lemma 8 (choosing $\mu = \mu^*$ and $\Psi = \Psi^*$) and Lemma 7 (choosing $\eta = \mu^*$), we are able to summarize the design, and realize the control goal, which is presented in Theorem 1. Define $e_y(t) = y - y_m$ and $e_z(t) = z - z_m$.

Theorem 1. *For an uncertain plant model (7) that satisfies Assumptions 1 to 6 and for any $z_{cmd}(t)$ that is piecewise continuous, the adaptive SPR/LTR controller (11)(12)(13)(14)(16), with L_ρ as in (33) and S_1 as in (21), guarantees that i) the closed-loop system has bounded solutions, ii) $e_y(t) \to 0$ as $t \to \infty$ and iii) $e_z(t) \to 0$ as $t \to \infty$.*

3. LTR Properties

The observer parameter L_ρ as in (33) can replace the observer parameter in the baseline observer-based controller. The following Lemma shows that the resulting baseline controller approaches full-state LTR asymptotically.

Lemma 9. *For a nominal plant model $\{A, B, C\}$ (without uncertainties Λ^* or Θ^*) satisfying Assumptions 1 to 4, suppose that a LQR controller with a parameter K has a loop gain at input $L_u^*(s)$ and a loop gain at output $L_o^*(s)$, and that the baseline observer-based controller (12)(13) with K and L_ρ as in (33), has loop gains $L_u(s)$ and $L_o(s)$; then as $\epsilon \to \infty$ or $\rho \to \infty$, i)*

$$L_u(s) \to L_u^*(s) \tag{36}$$

and ii)

$$L_o(s) \to C\left[L_o^*(s)\right]C^\dagger(s, \bar{B}) \tag{37}$$

where $C^\dagger(s, \bar{B}) \in \mathbb{R}^{n\times p}$ is a function of s and $\bar{B}$ satisfying $CC^\dagger(s, \bar{B}) = I_p$.

Remark 1. Since i) is a standard LTR result[9] and ii) holds for any LQG/LTR controllers using a squared-up $\bar{B}$, Lemma 9 implies that L_ρ retains the full-state LTR properties of a LQG/LTR controller. LQR controllers can be designed to have a $L_u^*(s)$ that yields good stability margins, and have a $L_o^*(s)$ that yields low output sensitivities at the integral loops (see Ref.[16] Chapter 2 and Chapter 5). As a result, Lemma 9 implies that once a large enough L_ρ is chosen, the stability margins of the baseline controller are guaranteed, and the output sensitivities at the integral loops can be tuned by designing $\bar{B}$ and K together, which is currently under investigation. However, one should be cautious to use a large L_ρ because $L_o^*(s)$ can have high output sensitivities at some other loops and so can $L_o(s)$.

Lemma 9 and Lemma 8 imply that the baseline controller and the adaptive controller can share a same observer and the controllers can switch between each other by simply turning u_{ad} on or off. When u_{ad} is off, the controller is denoted as the baseline SPR/LTR controller. The L_ρ design as in (33) has been preliminarily reported in Ref.[21]. This paper formally proves its SPR properties and its LTR properties.

C. Design Procedure

The overall control design can be summarized into the following step-wise procedure:

Step 1. Given a plant model $< A_p, B_p, C_p, C_{pz}, D_{pz} >$, check Assumptions 1 to 4;

Step 2. Add integral error states to the plant model and obtain $< A, B, C, C_z, D_z >$ using (9);

Step 3. Design a baseline observer-based controller (12)(13) and choose K and an observer parameter using the LQR and the LTR techniques, respectively;

Step 4. Design a μ^* using (23) and ϵ using (27), then design a nominal SPR pair L using Eq.(25) and S_1 using Eq.(21);

Step 5. Calculate Ψ^*_{max} using Eq.(32) and pick ρ using Eq.(34); then design a L_ρ using Eq.(33) and replace the observer gain in the baseline controller (13) with L_ρ;

Step 6. Design parameter adaptation (16) and add the adaptive control (14) to the baseline control (11).

Step 1 to Step 3 are conventional observer-based controller designs. Step 4 to Step 6 are for the adaptive component addition, which completes our adaptive SPR/LTR control design. It is noted that for both the baseline controller and the adaptive controller, the L_ρ design is independent from the K design. We can generally consider that K is designed for performance, and L_ρ is designed for stability.

D. Comparison with Other Adaptive Output-Feedback Controllers

Previous sections have presented the complete design of the proposed adaptive controller. The controller framework in Section A has been proposed in Ref.[16,21,22] but with different procedures for choosing L and S_1. We now compare our SPR/LTR method described in Section C with the previous approaches.

In order to carry out the comparison, we first return to the solution P of (18) and (19) for the choice of L_ρ as in (33) and S_1 as in (21). We rewrite the unique solution P to (18) and (19) as

$$P = \bar{C}^T(\bar{C}\bar{B})^{-1}\bar{C} + N^T P_I N \tag{38}$$

where $P_I > 0$ is defined in (29) (see proof of Lemma 6 and Lemma 8). P validates our SPR design.

An alternate procedure for choosing L and S_1, denoted as the adaptive observer-based LTR (OBLTR) control method, is presented in Ref.[16] (see Chapter 14). The procedure is presented as follows. A $\bar{B}$ is first designed using (20), then the weights

$$Q_v = Q_{v0} + \frac{v+1}{v}\bar{B}\bar{B}^T; \quad R_v = \frac{v}{v+1}R_{v0} \tag{39}$$

are chosen using arbitrary constant matrices $Q_{vo} > 0$ and $R_{v0} > 0$, and a sufficiently small scalar v. The following ARE is solved

$$P_v\bar{A}^T + \bar{A}P_v - P_vC^TR_v^{-1}CP_v + Q_v = 0. \tag{40}$$

for a unique SPD solution P_v. We choose $\bar{A}$ using (24) in Eq.(40), which is similar to Ref.[4], but with a bound that $0 < \mu^* < |\mu_{max}|$ to ensure SPR properties (see below). L is chosen to be L_v as

$$L_v = P_vC^TR_v^{-1}, \tag{41}$$

and S_1 is chosen to be $W_1 \in \mathbb{R}^{m\times p}$ as

$$WR_{v0}^{-\frac{1}{2}} = [W_1, W_2] \tag{42}$$

where $W \in \mathbb{R}^{p\times p}$ is designed as

$$W = U_wV_w, \quad U_w\Lambda_wV_w = svd(\bar{B}^TC^TR_{v0}^{\frac{1}{2}}) \tag{43}$$

where *svd* stands for singular value decomposition. Combined with the control architecture in Section A, the procedure from (39) to (43) completes the design of the adaptive OBLTR controller. The OBLTR design has been shown in Ref.[16] (see Theorem 13.2) to lead to

$$P_v = P_0 + O(v) \tag{44}$$

where $P_0 > 0$ is an unknown SPD matrix satisfying

$$P_0 C^T = \bar{B} W R_{\upsilon 0}^{\frac{1}{2}} \tag{45}$$

and $O(\upsilon)$ represents an unknown symmetric matrix which approaches to zero as $\upsilon \to 0$, which further leads to

$$L_\upsilon = P_\upsilon C^T R_\upsilon^{-1} \to \frac{1}{\upsilon} \bar{B} W R_{\upsilon 0}^{-\frac{1}{2}} \to \infty, \quad as\ \upsilon \to 0. \tag{46}$$

and therefore retains the LTR properties asymptotically (see Lemma 9 in this paper for a detail proof). Moreover, the OBLTR adaptive design has been shown in Ref. [16] (see Theorem 14.1) to lead to the existence of a υ that guarantees bounded reference tracking for a plant model (10) in the presence of uncertainties. The same OBLTR adaptive design has been shown in Ref. [21] (see Theorem 3 and its proof in Ref. [21], and combine with (24) and (40) in this paper) to lead to the existence of a non-zero υ that guarantees the SPR property of $\{(A + \mu^* I + \frac{1}{\mu^*} B\Psi^* - L_\upsilon C), B, W_1 C\}$ and in turn, guarantees asymptotic reference tracking.

Now we compare our SPR/LTR method with the OBLTR method. Both methods can produce a finite SPR pair of L and S_1. From Lemma 9, one can conclude that both methods lead to a L that retains the LTR properties of LQG/LTR controllers. However, the OBLTR method relies on the existence of a small υ for which the SPR properties are guaranteed. In practice, it may not be easy to determine how small υ needs to be. In contrast, our method (see (33)) provides a closed-form solution for both L and S_1.

An alternative procedure of designing L and S_1 based on the linear-matrix-inequality optimization techniques has been proposed in Ref. [22]. The parameter L is determined using a numerical procedure [22]; no closed-form solution for L or guaranteed LTR properties of the baseline controller are provided, unlike our SPR/LTR method.

V. Numerical Examples

This section presents the applications of the adaptive SPR/LTR controller on two VFA platforms. Section A presents the first platform, a simplified 3-wing VFA, whose low order model allows us to illustrate the LTR properties and the SPR properties of the controller. Section A introduces the application on the second platform, the Vulture VFA, whose high order model demonstrates the numerical stability of the proposed control design.

It should be noted that the adaptive SPR/LTR controller required Assumptions 1 to 6. It can be shown that all of these assumptions can be met by the VFA models of both platforms considered below. Of these, Assumption 4 is the most restrictive one, as it requires the VFA sensors to include measurements of linear velocities and angular velocities of the body components very close to actuators, and neglects actuator dynamics altogether.

A. Vertical Acceleration Tracking of 3-wing VFA

Consider a simple VFA comprised of three rigid wings with elastic pivot connections adjoining them [4]. The longitudinal and vertical dynamics of the 3-wing VFA is coupled with the dynamics of rotational movement of outer wings with respect to the center wing about the chord axis. The angle between the two wing planes is denoted as wing *dihedral* (η). A 7-state nonlinear model has been derived in Ref. [4] including the pitch mode, the phugoid mode, and the dihedral dynamics. The nonlinear model was trim at 30ft/sec airspeed, 40,000 ft altitude and different dihedrals, and the corresponding linearized models with respect to each dihedral were obtained [4]. Local stability analysis shows that when the dihedral is above 15°, the pitch mode becomes unstable [4].

We performed sensitivity analysis (using the method in Ref. [31] Chapter 9) on the linearized model and found that the pitch mode and the dihedral dynamics (pitch-dihedral dynamics) can be decoupled from the phugoid mode. Assuming that the airspeed is maintained by auto-thrust, we truncated the phugoid mode from the model and obtained a 4-state LTI model with states as $x_p = [\alpha, q, \eta, \dot{\eta}]$, where α is the angle of attack and q is the pitch rate. Measurements are vehicle vertical acceleration (A_z), and q. However, α, η and its rate $\dot{\eta}$ cannot be measured accurately and are not available for control. We want to use all three elevators δ_e unanimously (as 1 control) to achieve the tracking of a vertical acceleration command of the center wing while keeping the dihedral regulated. For Step 1, we obtained a

plant model for $\eta = 10^\circ$ as

$$\begin{bmatrix} \dot{\alpha} \\ \dot{q} \\ \dot{\eta} \\ \ddot{\eta} \\ A_z \end{bmatrix} = \begin{bmatrix} -4.104 & 1.013 & 0.193 & 0.100 & 0 \\ -54.04 & 0.255 & 1.845 & 21.41 & 0 \\ 0 & 0 & 0 & 1 & 0 \\ 0.044 & 0.819 & -0.075 & -6.518 & 0 \\ -123.12 & 0 & 0 & 0 & 0 \end{bmatrix} \begin{bmatrix} \alpha \\ q \\ \eta \\ \dot{\eta} \\ V_z \end{bmatrix} + \begin{bmatrix} -0.795 \\ 5.991 \\ 0 \\ 0.195 \\ -23.84 \end{bmatrix} \delta_e \tag{47}$$
$$y = \begin{bmatrix} q \\ V_z \end{bmatrix} = \begin{bmatrix} 0 & 1 & 0 & 0 & 0 \\ 0 & 0 & 0 & 0 & 1 \end{bmatrix} x.$$

We have integrated A_z into V_z, the climb rate measurement, for command tracking. Eq.(47) is $\{A, B, C\}$ by Step 2. The pitch mode is stable for this trim. Before control design, let's consider the uncertainties in the plant model. First, there might be a control surface damage up to 90% (Λ^*). Second, since the outer elevators are connected to the outer wings, their control effectiveness is a function of η. To learn the function form, we obtained the linearized model for $\eta = 16^\circ$. Compared with that of $\eta = 10^\circ$ in (47), the change in the control effectiveness can be approximated as $\Lambda^*\Theta^{*T}x$ added to u, which leads to the following uncertain model

$$\begin{aligned} \dot{x} &= (A + B\Lambda^*\Theta^{*T})x + B\Lambda^* u \\ \Lambda^* = 0.1; \quad \Theta^{*T} &= \begin{bmatrix} -31.94 & 0.91 & 9.1 & -9.28 & 0 \end{bmatrix}. \end{aligned} \tag{48}$$

Λ^* and Θ^* are unknown to control design. The pitch mode of (48) is unstable and therefore loosing control effectiveness imposes a threat to stability. The uncertain plant model (48) belongs to the class of models in (10) satisfying Assumptions 1 to 6.

We now proceed to control design based on (48) with uncertain Λ^* and Θ^* . The classical adaptive approach can only handle a minimum-phase square systems [12,13], which is inapplicable here since the SISO transfer function from δ_e to V_z is non-minimum-phase. The proposed controller in this paper can be applied here since the additional q measurement makes (47) a non-square minimum-phase plant. Now we present our control design step by step. Step 3 used the LQR technique with a penalty $diag\begin{bmatrix} 1 & 1 & 0.01 & 0.01 & 0.01 \end{bmatrix}$ on the states and a penalty 10 on the input, which yielded

$$K = \begin{bmatrix} -0.9154 & 0.2534 & 0.1382 & 0.5614 & -0.0316 \end{bmatrix}. \tag{49}$$

The following matrices are produced in Step 4:

$$B_2 = \begin{bmatrix} 0 & 0.9699 & 0 & 0 & 0.2437 \end{bmatrix}^T \tag{50}$$

$$S = \begin{bmatrix} 0.2437 & -0.9699 \\ 0.9699 & 0.2437 \end{bmatrix}. \tag{51}$$

We used (42) to design S. It was confirmed that $\{A, \bar{B}, \bar{C}\}$ remains minimum-phase and $\bar{C}\bar{B} = (\bar{C}\bar{B})^T > 0$. Using Eq.(25) with $\bar{A} = A$ and $\epsilon = 10$ yielded

$$L = \begin{bmatrix} -4.116 & 6.949 \\ 41.94 & -52.53 \\ 0 & 0 \\ 1.011 & -1.708 \\ -120.74 & 208.44 \end{bmatrix} \tag{52}$$

$$S_1 = \begin{bmatrix} 0.2437 & -0.9699 \end{bmatrix}. \tag{53}$$

A P was found using Eq.(38) as

$$P = \begin{bmatrix} 82.71 & 0.689 & -139.7 & -19.21 & -2.741 \\ * & 0.9489 & -1.372 & -0.2030 & 0.2036 \\ * & * & 963.9 & 140.3 & 5.462 \\ * & * & * & 26.70 & 0.8079 \\ * & * & * & * & 0.1898 \end{bmatrix} \tag{54}$$

where $*$ represents symmetric elements. Quick examination confirmed that $P > 0$, and that P, L and S_1 satisfy Eq.(18) and Eq.(19), which validates the SPR properties of $\{(A - LC), B, S_1C\}$.

We assumed the uncertainties Λ^* and Θ^* can be bounded by $\Lambda^*_{max} = 1.1$ and $\Theta^*_{max} = 32$. Also, it was assumed that $\Phi(x_p) = x_p$ and therefore $l_\phi = 1$ and $\Psi^* = \Lambda^*\Theta^*$. Step 5 produced $\Psi^*_{max} = 11.9$ and $\rho^* \approx 4.92$, and therefore $\rho = 5$ is chosen and

$$L_\rho = \begin{bmatrix} -5.084 & 10.80 \\ 53.94 & -80.40 \\ 0 & 0 \\ 1.249 & -2.655 \\ -148.6 & 324.37 \end{bmatrix}. \tag{55}$$

The same P as in (54) guarantees the SPR properties of $\{(A + B\Lambda^*\Theta^* - L_\rho C), B, S_1 C\}$. This completes our SPR/LTR control design.

For comparison, the design using the OBLTR method (41) with $v = 0.0006$, $Q_{v0} = I$ and $R_{v0} = 10000I$ was also obtained as

$$L_v = \begin{bmatrix} -3.200 & 12.41 \\ 42.07 & -94.32 \\ 0.286 & -0.109 \\ 1.325 & -3.187 \\ -94.32 & 382.3 \end{bmatrix} \tag{56}$$

$$W_1 = \begin{bmatrix} 0.2437 & -0.9699 \end{bmatrix}. \tag{57}$$

To validate that the pair of L_v and W_1 produces an SPR $\{(A - L_v C), B, W_1 C\}$, we propose a semidefinite programming procedure (see Ref.[32,33]) that can be added to the OBLTR method: reduce v until a P_0^* can be found using

$$\begin{aligned} &min && Tr(\bar{W}_p^T \bar{W}_p) \\ &s.t. && \bar{W}_p > 0, \\ & && (A - L_v C)^T P_0^* + P_0^*(A - L_v C) < 0, \\ &and && P_0^* \in \overline{\mathscr{P}}, \\ &where && \overline{\mathscr{P}} := \{P > 0 \mid P = \bar{C}_w^T(\bar{C}_w \bar{B})^{-1}\bar{C}_w + N^T \bar{W}_p N, \quad \bar{W}_p > 0\} \end{aligned} \tag{58}$$

where Tr stands for the trace of a matrix and $\bar{C}_w = W R_{v0}^{\frac{1}{2}} C$. A parser, Yalmip,[34] was used to execute the program (58) with L_v as in (56) and W as in (57). A P_0^* was found as

$$P_0^* = \begin{bmatrix} 41.72 & 0.3328 & -1.5328 & -2.162 & -1.325 \\ * & 0.9457 & -0.0177 & -0.0194 & 0.2161 \\ * & * & 16.35 & 2.881 & 0.0703 \\ * & * & * & 1.215 & 0.0772 \\ * & * & * & * & 0.1398 \end{bmatrix} \tag{59}$$

which guarantees that $\{(A - L_v C), B, W_1 C\}$ is SPR. However, to guarantee that $\{(A + B\Lambda^*\Theta^* - L_v C), B, W_1 C\}$ is SPR, we need to further reduce v, for which the OBLTR method does not have a closed-form solution, whereas our SPR/LTR method does.

Figure 2 shows that the two designs were able to constrain the phase of the target SPR transfer function within ± 90 degree, which is a necessary condition of SPR properties. Figure 3 shows that the uncertainties in (47) broke the ± 90 phase condition, and that replacing L with L_ρ was able to recover the phase condition. It is observed in Figure 4 that the loop gain at input of the baseline SPR/LTR controller almost overlays that of the LQR controller in terms of both phase and magnitude. The gain margin and phase margin of the baseline controller is $[-44, 42]$dB and ± 59 deg, respectively. Also shown in the Figure 4 is the baseline OBLTR controller. Both baseline controllers, as well as the LQR controller, have adequate stability margins since their $L_u(s)$ all avoid the unit circle around -1.

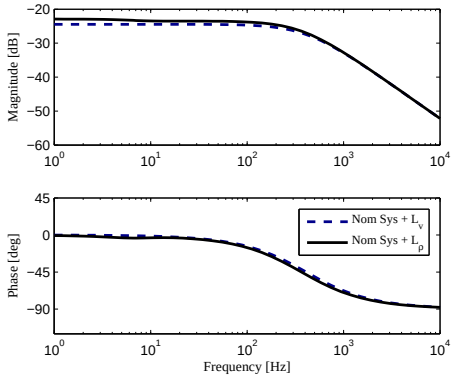

Figure 2. The Bode plot of the SPR system $\{(A - LC), B, S_1C\}$ for the 3-wing VFA model using the SPR/LTR observer parameter $L = L_\rho$; the design $L = L_v$ for a OBLTR controller is also presented for comparison

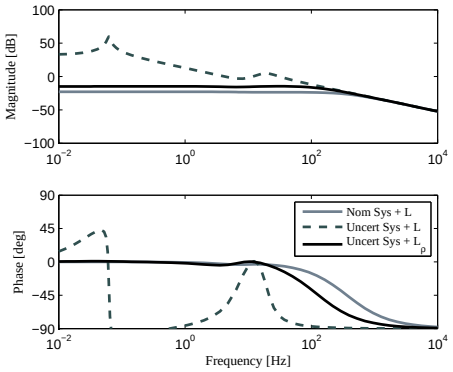

Figure 3. L_ρ in the baseline controller is able to recover the phase condition of $\{(A + B\Lambda^*\Theta^* - L_\rho C), B, S_1C\}$ with unknown Θ^* and Λ^* present in the 3-wing VFA model

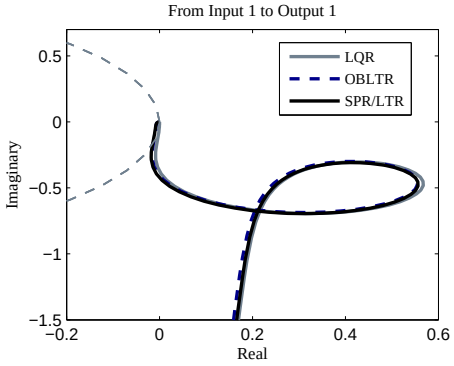

Figure 4. The Nyquist plot of the loop gain at input, $L_u(s)$, of the baseline controllers, compared with that of the LQR controller on the 3-wing VFA model (the gray dash line is a part of the unit circle around -1)

The uncertain VFA model (48) with different η was simulated with the baseline SPR/LTR controller and with the adaptive addition. An actuator model with a bandwidth 10 rad/sec was added in each simulation. The nominal case with the 10° dihedral plant model is shown in Figure 5a. Both controllers were able to guide the aircraft following an A_z command and eventually achieved zero tracking error. Only small amount of control and control rates were used. The same controllers were used to control the 16° dihedral, whose results are shown in Figure 5b. In this case, the baseline controller was not able to suppress the unstable pitch mode, while the adaptive controller was. Figure 5c shows the adaptive controller was robust in the presence of noise and random disturbance (white noise with 0.15 standard deviation) in all input and measurement channels.

The parameter trajectories are shown in Figure 10. After four step commands, the parameters settled down to their steady states. If we freeze $\Theta(t)$ and $\Lambda^{-1}(t)$ at different moments and use these instantaneous values in u_{ad} (14), the resulting closed-loop systems represent the "snapshots" of the adaptive system in the time history. The examination in frequency domain confirmed that these "snapshot" closed-loop systems approach to the nominal closed-loop system as time evolves, as shown in Figure 6b.

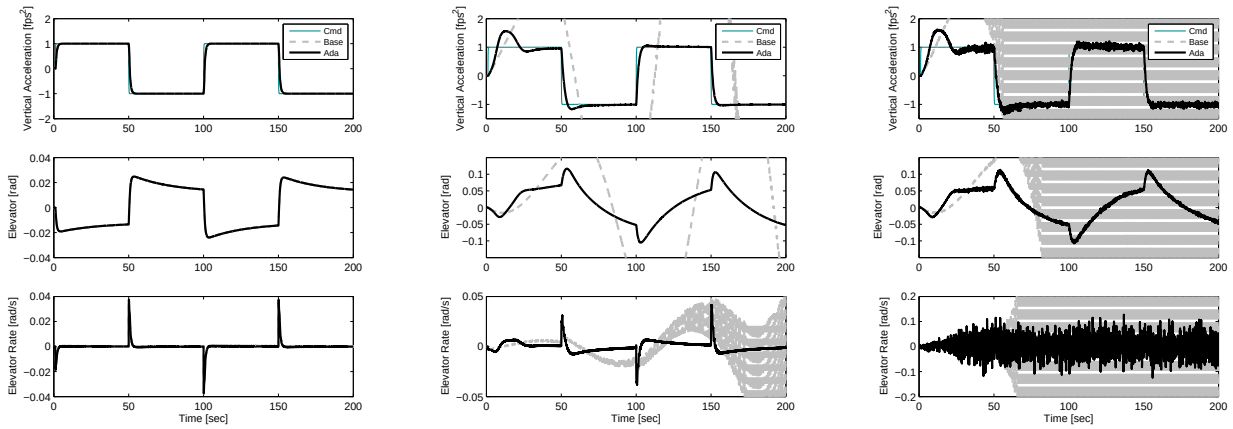

a) The nominal case b) The uncertain case c) The uncertain case with noise and disturbance

Figure 5. The simulation results of the vertical acceleration tracking of the 3-wing VFA using the adaptive output-feedback controller, compared with the baseline SPR/LTR controller

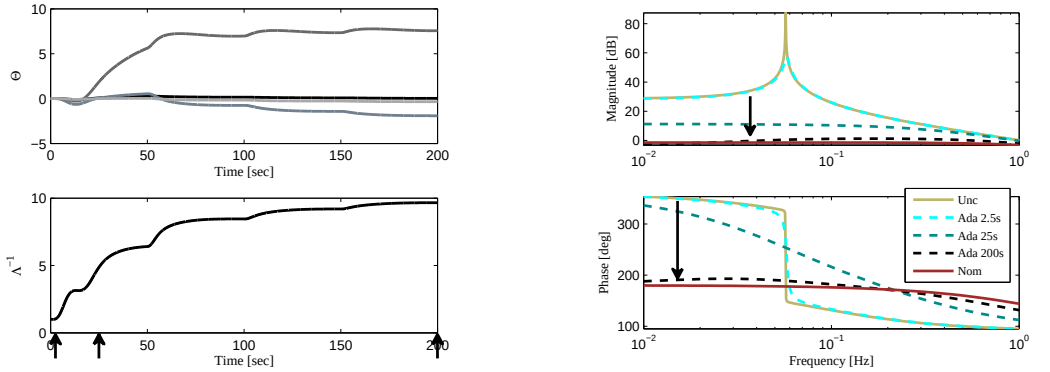

a) The parameter trajectory b) The "snapshots" of the closed-loop system at three moments marked on (a)

Figure 6. The parameter trajectory in time domain and the "snapshots" of the closed-loop systems in frequency domain on the 3-wing VFA model for the run in Figure 5b

B. Vulture VFA Bank-To-Turn Control

The previous example of 3-wing VFA represents building blocks of the Vulture VFA. One can consider the wings of the Vulture as hundreds of 3-wing segments adjoined together. The huge wings are in junction with 4 long booms in the middle of wingspan and 2 end devices at the tips. The control model for the VFA is a non-strictly proper LTI model with 707 states, 21 control inputs and 212 outputs, representing the VFA trim at a nominal HALE flight condition at an airspeed of 34.6 ft/sec, an altitude of 66,000 ft, and with zero dihedral[6]. The 21 inputs includes 15 engine propellers evenly placed across the wingspan and 6 tail elevators at the end of each boom (see Ref.[6] for details). If dividing the 707 states into three groups, i.e. rigid body dynamics states x_{RB} for 6 vehicle degrees of freedom, 340 flexible positions x_{flex}, and 340 flexible velocities v_{flex}, the Vulture model manifests itself in the following block matrix form:

$$\begin{bmatrix} \dot{x}_{RB} \\ \dot{v}_{flex} \\ \dot{x}_{flex} \end{bmatrix} = \begin{bmatrix} \times & \times & * \\ \times & o\backslash o & \times \\ 0 & I & 0 \end{bmatrix} \begin{bmatrix} x_{RB} \\ v_{flex} \\ x_{flex} \end{bmatrix} + \begin{bmatrix} 0 \\ \times \\ 0 \end{bmatrix} u + \begin{bmatrix} * \\ \times \\ 0 \end{bmatrix} \dot{u} + \begin{bmatrix} * \\ \times \\ 0 \end{bmatrix} \ddot{u} \tag{60}$$
$$y_p = C_p x + D_p u + D_1 \dot{u} + D_2 \ddot{u}$$

where $\times$ represents dense entries, $*$ represents sparse entries and $o\backslash o$ represents diagonal entries. Some observations are made. First, the flexible modes are strongly coupled with rigid-body dynamics. Second, the control u only acts on flexible component. Third, there are control rate $\dot{u}$ and control acceleration $\ddot{u}$ effects, which represent aero-

elastic-coupling between unsteady aerodynamics and flexible effects of boom. These features imposes great control challenges.

The desired maneuver is to bank the VFA to turn (BTT). The controller needs to force the VFA to follow a roll angle while keeping the aircraft oriented. In order to do so, we used tails to roll the aircraft and used engine thrusts to keep the side slip angle at zero. The 6 tails were divided into two groups, 3 on right and 3 on left. Same magnitude but opposite sign of movement was issued to each group. The 15 engines were also divided into two groups with an even number of engines in each group. This treatment reduced the number of input to 2, one for engine and one for tail. B_p was suitably treated. The control rate and acceleration effects were ignored in the design stage and were brought back in the simulation.

The high-order nature of the model necessitates a state-space reduced-order approach. Using the balanced realization method[35], we obtained a 80-state model which preserves the frequency domain performance of the model at low frequencies (lower than 100Hz)[20]. Using sensitivity analysis on the reduced model (see Ref.[31] Chapter 9), we determined the 12 independent outputs that yields CB full rank. They are roll rate, pitch rate, yaw rate, longitudinal, lateral and vertical accelerations at the wingroot, and corresponding angular rates and accelerations measured at tail 2. The measurements at tail 2 are used to satisfy Assumption 4. After integrating non-strictly proper outputs, we obtained a strictly proper LTI model with $n_p = 92$ states, $m = 2$ inputs and $p_p = 12$ outputs.

We designed the adaptive controller based on the reduced-order model. Quick examination confirmed that the reduced-order model satisfies Assumptions 2 to 4. The effects of the dihedral drift and actuator anomalies were modeled by $\Theta^*\Phi(x_p)$ and Λ^*, respectively. Assumptions 5 and 6 are satisfied with $l_\phi = 10$. The state-feedback gain K was found using a penalty of 1.45 on each of the outputs and a penalty of 1 on each of the inputs. The gain matrix L_ρ and S_1 were found with $\mu^* = 0.01$, $\epsilon = 50$ and $\rho = 10$. To show the robustness of the baseline controller, the "Gang-of-Six"[36] is examined in Figure 7. The ideal LQR controller is also shown in the figure for comparison. The figure shows that the loop gain at input $L_u(s)$ of the baseline SPR/LTR controller almost recovers that of a LQR; gain margin and phase margin are found to be $[-5.04, 4.75]$dB and ± 25 deg, respectively. The crossover frequency of $L_u(s)$ is around 0.1 rad/sec. The output sensitivity function $S_o(s)$ (only the integral loops are shown in the figure) has low magnitude. The magnitude of the noise-to-control transfer function gradually rolls off at high frequencies.

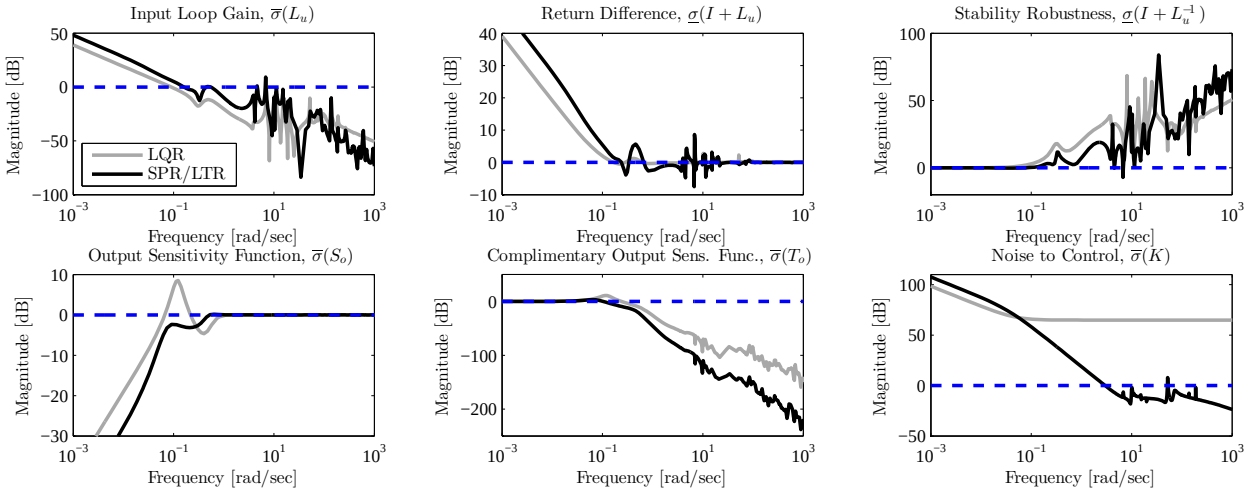

Figure 7. The frequency domain analysis of the closed-loop system using the baseline SPR/LTR controller on the Vulture VFA model, compared with a LQR

Three controllers, i.e. the LQR controller, the baseline SPR/LTR controller, and the adaptive SPR/LTR controller were simulated on the original Vulture model. We included control rate and control acceleration effects in the simulation. Also, second-order actuators with a natural frequency of 50 rad/sec and a damping ratio of 0.6 were introduced to all control channels. Magnitude saturation of ± 10 deg and rate saturation of ± 40 deg/s were imposed on the tail. Magnitude saturation of $[-50, 40]$ lbs and rate saturation of ± 20 lbs/s were imposed on the engine. For additional robustness, a projection algorithm[37] was incorporated into the adaptation law (16)

$$\begin{aligned} \dot{\Theta}(t) &= proj[\Theta;\ \vartheta, \epsilon;\ \Gamma_\theta \Phi(x_{mp}) e_y^T S_1^T sign(\Lambda)] \\ \dot{\Lambda}^{-1}(t) &= proj[\Lambda^{-1};\ \vartheta, \epsilon;\ -\Gamma_\lambda u_{bl} e_y^T S_1^T sign(\Lambda)] \end{aligned} \tag{61}$$

to bound $\Theta(t)$ and $\Lambda^{-1}(t)$ without altering the stability and tracking results in Theorem 1. The projection parameters were set as $\Gamma_\theta = 0.01I$, $\Gamma_\lambda = 0.01I$ $\vartheta = 10^{-3}I$ and $\varepsilon = 10^{-3}I$.

The simulation results of the nominal plant model (without uncertainty) is shown in Figure 9a. All three controllers had exactly the same performance and achieve perfect command tracking for both roll angle and side slip angle. The non-minimum-phase behavior in the responses were caused by the flexible effect of booms and by the interaction between wing sections. Figure 9b shows the performance of controllers in the presence of uncertainties. Before time started, we let the aircraft settle down to a different dihedral angle, emulating turbulence-driven dihedral drift. 10ft dihedral on the outer wing was present at $t = 0$, as shown in the wing shape evolution Figure 8b. Correspondingly, $\Phi(x)$ was a parabolic function with suitable coefficients to represent the concave wingshape. Also, there was a power surge in all actuators with $\Lambda^* = 1.5$. In the presence of uncertainties, neither LQR or the baseline SPR/LTR controller was able to stabilize the aircraft, as shown in the Figure 9a and 9b, . On the other hand, the adaptive controller not only stabilized the aircraft but also recovered the reference performance (as that in Figure 9a). The adaptive controller did so by actively reducing its control gains and therefore using much less control rates than the other two controllers.

Figure 9c shows the same uncertain case with gust wind (white noise with a standard deviation of 10^{-3}) and measurement noise (white noise with a standard deviation of 10^{-3}) in all 12 measurement channels. It is shown in the figure that adaptive controller is robust under these adversities. Figure 10 shows the parameter trajectories in this simulation. The 89 adaptive parameters settled down to steady-state values after three step commands. The smooth trajectories show that the noise and disturbance was attenuated by the controller. Figure 8a shows the flight path and attitude of the VFA in 3D space. The rendered aircraft represents the center section of the VFA, and the roll angle of the wing section in the figure only represents the local roll angle very close to the center wingroot (only about 1 deg). The actual dihedral shape of the entire wingspan was found by recording the flexible positions of the wing and is shown in Figure 8b. The dihedral was trimmed at a parabolic shape at $t = 0$ sec and ended at a nonlinear form at $t = 80$ sec. After that it gradually returned to the trim value (not shown in the figure).

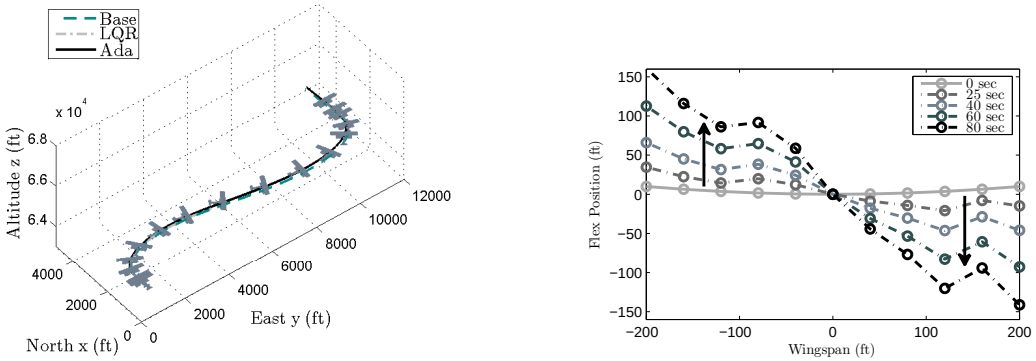

a) The flight path and attitude of the center wing (not in scale)

b) The wing dihedral shape evolution (rear view)

Figure 8. The flight path and dihedral shape of the VFA in the BTT maneuver, controlled by the adaptive SPR/LTR controller.

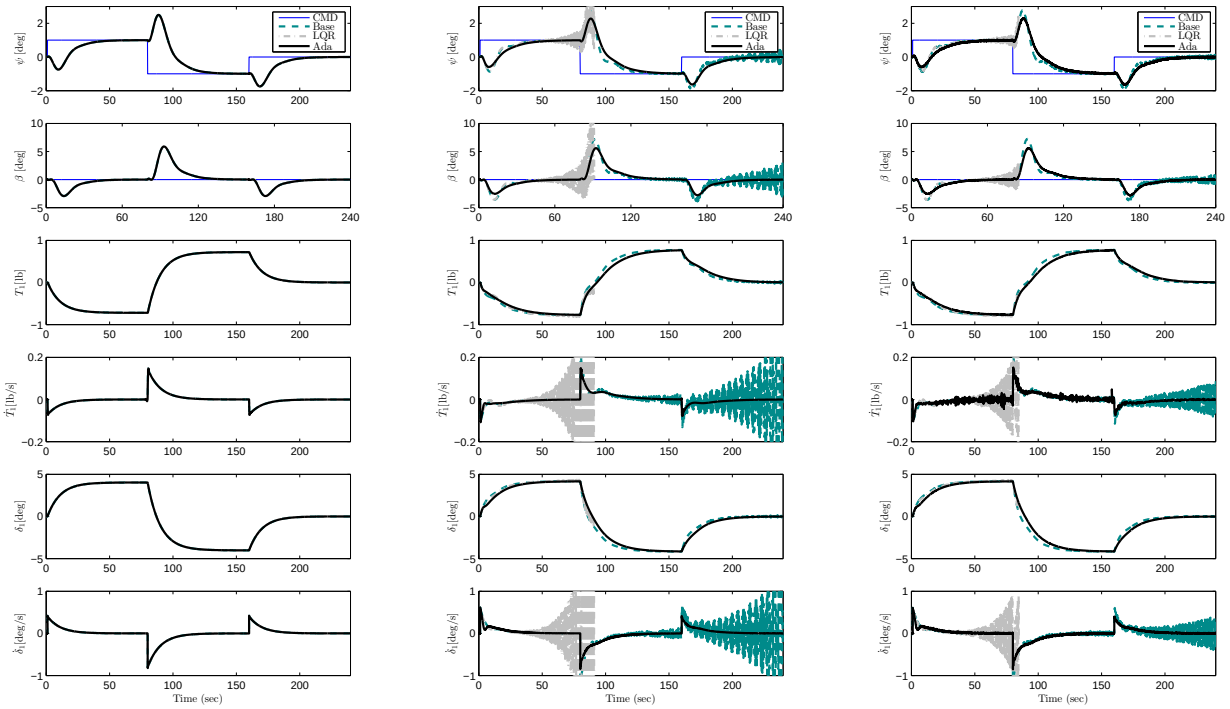

a) The nominal case b) The uncertain case c) The uncertain case with noise and disturbance

Figure 9. The tracking of roll angle (ψ) and side-slip angle (β) in the BTT maneuver of the VFA through thrust (T_1) and tail (δ_1) using the adaptive SPR/LTR controller, compared with the baseline controller and a LQR.

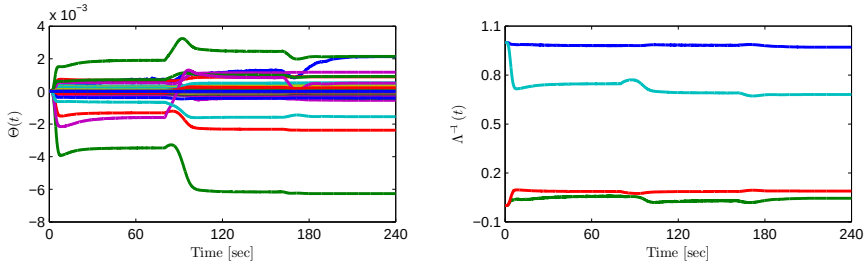

Figure 10. The adapted parameters settle down to steady-state values after three step commands of BTT on the Vulture model

VI. Conclusions

VFA imposes a great challenge for existing control technologies because the autonomous systems are required to endure a large amount of uncertainties and anomalies in a high-altitude long-endurance flight. The control problem is even more difficult since the flexible modes of aircraft cannot be measured despite their critical effects on the flight dynamics. To tackle the challenge, this paper proposes a new model reference adaptive output-feedback control solution, denoted as the adaptive SPR/LTR controller, for a class of MIMO plants with more outputs than inputs. The proposed adaptive controller is applied on two typical VFA models and the adaptive systems achieve asymptotic reference tracking.

An important feature of the adaptive controller is that it shares the same minimal observer with a baseline observer-based controller and therefore it can be constructed as an additional component to the baseline. Moreover, the observer also doubles as a closed-loop reference model, and therefore the number of integrators required for implementation is greatly reduced. The observer parameters are redesigned to retain the desirable LTR properties, which produces a robust baseline controller, and in addition, satisfy an underlying SPR condition, which guarantees global asymptotic

reference tracking in the presence of uncertainties. Current work is focused on relaxing the requirement regarding the placement of sensors and actuators as in Assumption 4.

Acknowledgments

The work presented in this paper was supported by the Boeing Strategic University Initiative. The authors would like to thank Eugene Lavretsky of The Boeing Company for several highly useful discussions.

References

[1]Langford, J., "The Daedalus project - A summary of lessons learned," American Institute of Aeronautics and Astronautics, 1989.

[2]Shearer, C. and Cesnik, C., "Nonlinear Flight Dynamics of Very Flexible Aircraft," *AIAA Atmospheric Flight Mechanics Conference and Exhibit*, 2005.

[3]Su, W. and S., C. E. C., "Dynamic Response of Highly Flexible Flying Wings," *AIAA Journal*, Vol. 49, No. 2, 2011, pp. 324–339.

[4]Gibson, T., Annaswamy, A., and Lavretsky, E., "Modeling for Control of Very Flexible Aircraft," Guidance, Navigation, and Control and Co-located Conferences, American Institute of Aeronautics and Astronautics, 2011.

[5]Noll, T. E., Brown, J. M., Perez-Davis, M. E., Ishmael, S. D., Tiffany, G. C., and Gaier, M., "Investigation of the Helios Prototype Aircraft Mishap Volume I: Mishap Report," *NASA*, 2004.

[6]Gadient, R., Wise, K., and Lavretsky, E., "Very Flexible Aircraft Control Challenge Problem," Guidance, Navigation, and Control and Co-located Conferences, American Institute of Aeronautics and Astronautics, 2012.

[7]Rynaski, E., "Flight control synthesis using robust output observers," American Institute of Aeronautics and Astronautics, 1982.

[8]Thompson, C., Coleman, E., and Blight, J., "Integral LQG controller design for a fighter aircraft," American Institute of Aeronautics and Astronautics, 1987.

[9]Doyle, J. and Stein, G., "Multivariable feedback design: Concepts for a classical/modern synthesis," *Automatic Control, IEEE Transactions on*, Vol. 26, No. 1, 1981, pp. 4–16.

[10]Wise, K. and Lavretsky, E., "Asymptotic Properties of LQG/LTR Controllers in Flight Control Problems," *AIAA Guidance, Navigation, and Control Conference*, 2012.

[11]Maciejowski, J. M., *Multivariable feedback design*, Addison-Wesley, Wokingham, England; Reading, Mass., 1989.

[12]Narendra, K. S. and Annaswamy, A. M., *Stable adaptive systems*, Dover Publications, 2004.

[13]Tao, G., *Adaptive control design and analysis*, Wiley-Interscience, Hoboken, N.J., 2003.

[14]Morse, A. S., "Parameterizations for multivariable adaptive control," *Proceedings of the 20th IEEE Conference on Decision and Control including the Symposium on Adaptive Processes*, IEEE, New York, NY, USA, 1981, pp. 970–972.

[15]Singh, R. P. and Narendra, K. S., "Prior information in the design of multivariable adaptive controllers," *IEEE Transactions on Automatic Control*, Vol. AC-29, No. 12, 1984, pp. 1108.

[16]Lavretsky, E. and Wise, K. A., *Robust and adaptive control [electronic resource] : with aerospace applications*, Springer, London ; New York, 2013.

[17]Gibson, T., Annaswamy, A., and Lavretsky, E., "Improved Transient Response in Adaptive Control Using Projection Algorithms and Closed Loop Reference Models," Guidance, Navigation, and Control and Co-located Conferences, American Institute of Aeronautics and Astronautics, 2012.

[18]Gibson, T. E., Annaswamy, A. M., and Lavretsky, E., "Closed-Loop Reference Models in Adaptive Control: Stability, Robustness and Performance," .

[19]Gibson, T. E., Annaswamy, A. M., E., and Lavretsky, "Output Feedback Adaptive Control with Closed-Loop Reference Models," *European Control Conference*, 2013.

[20]Qu, Z., Lavretsky, E., and Annaswamy, A. M., "An Adaptive Controller for Very Flexible Aircraft," American Institute of Aeronautics and Astronautics, 2013.

[21]Gibson, T. E., Qu, Z., Annaswamy, A. M., and Lavretsky, E., "Adaptive Output Feedback based on Separation Principle and Closed-loop Reference Models," *IEEE Transactions Automatic Control (submitted 2013)*.

[22]Wiese, D. P., Annaswamy, A. M., Muse, J. A., Bolender, M. A., and Lavretsky, E., "Adaptive Output Feedback Based on Closed-Loop Reference Models for Hypersonic Vehicles," *AIAA Guidance, Navigation, and Control Conference (To Appear)*, American Institute of Aeronautics and Astronautics, 2015.

[23]MacFarlane, A. G. J. and Karcanias, N., "Poles and zeros of linear multivariable systems : a survey of the algebraic, geometric and complex-variable theory," *International Journal of Control*, Vol. 24, No. 1, 1976, pp. 33–74.

[24]Kouvaritakis, B. and MacFarlane, A. G. J., "Geometric approach to analysis and synthesis of system zeros. II. Non-square systems," *International Journal of Control*, Vol. 23, No. 2, 1976, pp. 167–181.

[25]Kouvaritakis, B. and MacFarlane, A. G. J., "Geometric approach to analysis and synthesis of system zeros. I. Square systems," *International Journal of Control*, Vol. 23, No. 2, 1976, pp. 149–156.

[26]Huang, C. H., Ioannou, P. A., Maroulas, J., and Safonov, M. G., "Design of strictly positive real systems using constant output feedback," *Automatic Control, IEEE Transactions on*, Vol. 44, No. 3, 1999, pp. 569–573.

[27]Weiss, H., Wang, Q., and Speyer, J. L., "System characterization of positive real conditions," *IEEE Transactions on Automatic Control*, Vol. 39, No. 3, 1994, pp. 540–544.

[28]Yu, J.-t., Chiang, M.-L., and Fu, L.-C., "Synthesis of static output feedback SPR systems via LQR weighting matrix design," *Decision and Control (CDC), 2010 49th IEEE Conference on*, 2010, pp. 4990–4995.

[29]Misra, P., "A computational algorithm for squaring-up. I. Zero input-output matrix," *Proceedings of 1992 31st IEEE Conference on Decision and Control*, IEEE, New York, NY, USA, 1992, pp. 149–150.

[30]Qu, Z., Wiese, D., Lavretsky, E., and Annaswamy, A. M., "Squaring-Up Method In the Presence of Transmission Zeros," *19th World Congress, The International Federation of Automatic Control*.

[31]Durham, W., *Aircraft Dynamics and Control*, 2013.

[32]Vandenberghe, L. and Boyd, S., "Semidefinite programming," *SIAM Review*, Vol. 38, No. 1, 1996, pp. 49–95.

[33]Parrilo, P. A., "Structured semidefinite programs and semialgebraic geometry methods in robustness and optimization," 2000.

[34]Lofberg, J., "YALMIP : a toolbox for modeling and optimization in MATLAB," *Computer Aided Control Systems Design, 2004 IEEE International Symposium on*, 2004, pp. 284–289.

[35]Moore, B., "Principal component analysis in linear systems: Controllability, observability, and model reduction," *IEEE Trans.Automat.Contr.IEEE Transactions on Automatic Control*, Vol. 26, No. 1, 1981, pp. 17–32.

[36]Astrom, K. J. and Murray, R. M., *Feedback systems : an introduction for scientists and engineers*, Princeton University Press, Princeton, 2008.

[37]Lavretsky, E. and Gibson, T. E., "Projection Operator in Adaptive Systems," *arXiv:1112.4232*.

Appendix

Proof of Lemma 5

Proof. The goal is to show $e_x(t) \to 0$ as $t \to \infty$. Since we have designed an SPR pair L and S_1 such that $\{(A - LC), B, S_1C\}$ is SPR, there exists a $P = P^T > 0$ such that Eq.(18) and Eq.(19) holds for a $Q > 0$. We propose a Lyapunov function candidate using the P as

$$V = e_x^T P e_x + Tr(\widetilde{\Lambda}^T \Gamma_\lambda^{-1} \widetilde{\Lambda} |\Lambda^*|) + Tr(\widetilde{\Theta}^T \Gamma_\theta^{-1} \widetilde{\Theta} |\Lambda^*|) > 0 \tag{62}$$

where Tr stands for the trace of a matrix. Using Eq.(15), V has a derivative as

$$\begin{aligned}\dot{V} &= e_x^T((A - L_\rho C)^T P + P(A - L_\rho C))e_x + 2e_x^T PB\Lambda^* \Theta^{*T}[\Phi(x_p) - \Phi(x_{mp})] \\ &\quad + 2e_x^T PB\Lambda^* \widetilde{\Lambda}^T u_{bl} - 2e_x^T PB\Lambda^* \widetilde{\Theta}^T \Phi(x_{mp}) + 2Tr(\widetilde{\Lambda}^T \Gamma_\lambda^{-1} \dot{\widetilde{\Lambda}} |\Lambda|) + 2Tr(\widetilde{\Theta}^T \Gamma_\theta^{-1} \dot{\widetilde{\Theta}} |\Lambda|) \qquad (63) \\ &= e_x^T((A - L_\rho C)^T P + P(A - L_\rho C))e_x + 2e_x^T PB\Lambda^* \Theta^{*T}[\Phi(x_p) - \Phi(x_{mp})] \\ &\quad + 2e_x^T[PB - C^T S_1^T]\Lambda^* \widetilde{\Lambda}^T u_{bl} - 2e_x^T[PB - C^T S_1^T]\Lambda^* \widetilde{\Theta}^T \Phi(x_{mp}). \qquad (64)\end{aligned}$$

To achieve (64), we used the property of trace and adaptation law (16). By far, the derivation is general for $\Theta^* \neq 0$. For the special case $\Theta^* = 0$, we choose $\Theta(t) \equiv 0$, then $\widetilde{\Theta}(t) \equiv 0$. Also, $L = L_\rho$. As a result, the error model (15) has a form of (17). Then the derivative of Lyapunov function (64) becomes

$$\dot{V} = e_x^T((A - LC)^T P + P(A - LC))e_x + 2e_x^T[PB - C^T S_1^T]\Lambda^* \widetilde{\Lambda}^T u_{bl}. \tag{65}$$

Using Eq.(18) and Eq.(19) turns (65) into

$$\dot{V} = -e_x^T Q e_x \leq 0. \tag{66}$$

As a result, e_x, $\widetilde{\Lambda}$ and $\widetilde{\Theta}$ are bounded. Moreover, $\dot{V}$ exists and is bounded and Barbalet's Lemma implies $e_x(t) \to 0$ as $t \to \infty$, which proves ii). Consequently, the observer/CRM (13) approaches to a open loop reference model when $t \to \infty$ and its state trajectory x_m is bounded (by the design of K). This in turn implies x is bounded. It then can be concluded that all signals in the system are bounded, which proves i). □

Proof of Lemma 6

Proof. The proof follows the idea in Ref.[28], but uses a different approach. First, we will show that $\{(\bar{A} - LC), B, S_1C\}$ is SPR, where $\bar{A} = A + \mu^* I$. We note that $\{\bar{A}, \bar{B}, \bar{C}\}$ is minimum phase. A weight R^{-1} is chosen in (26) and a weight $\bar{Q}$ (different from Ref.[28]) is chosen as

$$\bar{Q} = -N^T H(\bar{C}\bar{B})^{-1}\bar{C} - \bar{C}^T(\bar{C}\bar{B})^{-1}H^T N + \epsilon \bar{C}^T \bar{C} + N^T Q_I N \tag{67}$$

where H is defined in (28) and ϵ is chosen in (27). N is the null space of $\bar{B}$ and M is the null space of $\bar{C}$ satisfying and $NM = I$. We will show that the finite constant ϵ chosen in inequality (27) guarantees $R^{-1} > 0$ and $\bar{Q} > 0$. $R^{-1} > 0$ because $\epsilon > \epsilon_1^*$ where ϵ_1^* is defined in (27). To show $\bar{Q} > 0$, it is equivalent to show that $T_{\bar{B}}^T \bar{Q} T_{\bar{B}} > 0$, where

$$T_{\bar{B}} = [M, \bar{B}] \tag{68}$$

is an invertible matrix. Examination on $T_{\bar{B}}^T Q T_{\bar{B}}$ yields

$$T_{\bar{B}}^T \bar{Q} T_{\bar{B}} = \begin{bmatrix} M^T \bar{Q} M & M^T \bar{Q} \bar{B} \\ \bar{B}^T \bar{Q} M & \bar{B}^T \bar{Q} \bar{B} \end{bmatrix} = \begin{bmatrix} I & -H \\ -H^T & \epsilon(\bar{C}\bar{B})\bar{C}\bar{B} \end{bmatrix} > 0. \tag{69}$$

The inequality is guaranteed to hold using Schur complement and the fact that $\epsilon > \epsilon_2^*$, where ϵ_2^* is defined in (27), and therefore $\bar{Q} > 0$ is guaranteed.

Propose a P as

$$P = \bar{C}^T (\bar{C}\bar{B})^{-1} \bar{C} + N^T P_I N \tag{70}$$

where $P_I > 0$ is the unique solution to Eq.(29) and therefore $P > 0$. We will show because of the L design in (25) and S_1 design in (21), the P as in (70) satisfies

$$(\bar{A} - LC)^T P + P(\bar{A} - LC) = -\bar{Q} - \bar{C} R^{-1} \bar{C} < 0 \tag{71}$$

and Eq.(19) simultaneously. First, let's show Eq.(71) holds. Using L as in (33) and the fact $P\bar{B} = \bar{C}^T$, Eq.(71) can be rewritten as

$$\{\oslash\} := (\bar{A} - \bar{B} R^{-1} \bar{C})^T P + P(\bar{A} - \bar{B} R^{-1} \bar{C}) + \bar{C}^T R^{-1} \bar{C} + \bar{Q}. \tag{72}$$

To show $\{\oslash\} = 0$, it is equivalent to show $T_{\bar{B}}^T \{\oslash\} T_{\bar{B}} = 0$. Examination on the block elements of $T_{\bar{B}}^T \{\oslash\} T_{\bar{B}}$ reveals

$$T_{\bar{B}}^T \{\oslash\} T_{\bar{B}} = \begin{bmatrix} M^T \{\oslash\} M & M^T \{\oslash\} \bar{B} \\ \bar{B}^T \{\oslash\} M & \bar{B}^T \{\oslash\} \bar{B} \end{bmatrix} = 0. \tag{73}$$

Eq.(73) holds since $\bar{C}M = 0$, $N\bar{B} = 0$, $P\bar{B} = \bar{C}^T$, $PM = N^T P_I$, R^{-1} is chosen in (26) and Eq.(29) holds. This proves Eq.(71). The choice of P as in (70) implies $P\bar{B} = \bar{C}^T$. Then proper partition as in Eq.(21) and (20) allows element-wise equality (19). This implies that $\{(\bar{A} - LC), B, S_1 C\}$ is SPR.

Now, we note that for any μ satisfying $0 \le \mu \le \mu^*$, $(\mu^* - \mu)P \ge 0$. Following (71), it is clear that

$$(A + \mu I - LC)^T P + P(A + \mu I - LC) = -\bar{Q} - \bar{C} R^{-1} \bar{C} - 2(\mu^* - \mu)P < 0. \tag{74}$$

Eq.(74) and Eq.(19) implies that $\{(A + \mu I - LC), B, S_1 C\}$ is SPR. Because ϵ is finite, L is finite. This completes the proof of Lemma 6.

An additional result, $\lambda_{min}(P) > 1$, will be used later and therefore is proved here. With the proposed solution P in (70), it can be shown that

$$T_{\bar{B}}^T \{P - I\} T_{\bar{B}} = \begin{bmatrix} P_I - M^T M & -M^T \bar{B} \\ -\bar{B}^T M & \bar{C}\bar{B} \end{bmatrix}. \tag{75}$$

Applying Schur complement shows that since P_I satisfies (30), $T_{\bar{B}}^T \{P - I\} T_{\bar{B}} > 0$ and therefore $P > I$. □

Proof of Lemma 7

Proof. Given that we have designed an SPR pair of L_ρ and S_1 for the system $\{(A + \eta I + \frac{1}{\eta} B\Psi^* - L_\rho C), B, S_1 C\}$ with some $\eta > 0$, there exist a $P > 0$ such that

$$(A + \eta I + \frac{1}{\eta} B\Psi^* - L_\rho C)^T P + P(A + \eta I + \frac{1}{\eta} B\Psi^* - L_\rho C) \quad = \quad -Q_\rho < 0 \tag{76}$$

and Eq.(19) hold simultaneously for a $Q_\rho > 0$. Without loss of generality, we assume $\lambda_{min}(P) \ge 1$, which can always be satisfied by scaling Q_ρ and S_1. For our solution of P, see the end of proof of Lemma 6.

A Lyapunov function V as in (62) is proposed using the P in Eq.(76)(19), and therefore $\dot{V}$ is as in Eq.(64). Since $\Theta^* \ne 0$, $\dot{e}_x$ is as in Eq.(15) and the second term of the right hand side of Eq.(64) is no longer zero. By Assumption 6, the non-zero term can be bounded as

$$\begin{aligned} e_x^T PB\Lambda^* \Theta^{*T} [\Phi(x_p) - \Phi(x_{mp})] &\le \left\| e_x^T PB\Lambda^* \Theta^{*T} \right\| l_\phi \left\| e_x \right\| \\ &\le \frac{l_\phi}{\sqrt{\eta}} \left\| e_x^T PB\Lambda^* \Theta^{*T} \right\| \left\| \sqrt{\eta} P^{\frac{1}{2}} e_x \right\| \\ &\le \frac{l_\phi^2}{4\eta} e_x^T PB\Lambda^* \Theta^{*T} \Theta^* \Lambda^* B^T P e_x + e_x^T \eta P e_x. \end{aligned} \tag{77}$$

Substituting the definition of Ψ^* (31) and Eq.(19) into Eq.(77) yields

$$e_x^T PB\Lambda^*\Theta^{*T}[\Phi(x_p) - \Phi(x_{mp})] \leq e_x^T \frac{1}{\eta} PB\Psi^* e_x + e_x^T \eta P e_x. \tag{78}$$

Using inequality (78), the derivative of Lyapunov function (64) can be bounded as

$$\begin{aligned}\dot{V} &\leq e_x^T((A - L_\rho C)^T P + P(A - L_\rho C))e_x + 2\left[e_x^T \frac{1}{\eta} PB\Psi^* e_x + e_x^T \eta P e_x\right] \\ &\quad + 2e_x^T[PB - C^T S_1^T]\Lambda^*\widetilde{\Lambda}^T u_{bl} - 2e_x^T[PB - C^T S_1^T]\Lambda^*\widetilde{\Theta}^T\Phi(x_{mp}) \qquad (79) \\ &= e_x^T((A + \eta I + \frac{1}{\eta}B\Psi^* - L_\rho C)^T P + P(A + \eta I + \frac{1}{\eta}B\Psi^* - L_\rho C))e_x \\ &\quad + 2e_x^T[PB - C^T S_1^T]\Lambda^*\widetilde{\Lambda}^T u_{bl} - 2e_x^T[PB - C^T S_1^T]\Lambda^*\widetilde{\Theta}^T\Phi(x_{mp}) \qquad (80)\end{aligned}$$

Substituting Eq.(76) and Eq.(19) turns Eq.(65) into

$$\dot{V} \leq -e_x^T Q_\rho e_x \leq 0. \tag{81}$$

Thus, Eq.(62) is indeed the Lyapunov function of the system. Following the last part of the proof of Lemma 5, it can be concluded that $e_x(t) \to 0$ as $t \to \infty$, which proves ii) and x, e_x, $\widetilde{\Lambda}$ and $\widetilde{\Theta}$ are bounded, which proves i). □

Proof of Lemma 8

Proof. We will show that with the L_ρ design (33), the P that guarantees the SPR properties of $\{(A + \mu I - LC), B, S_1 C\}$ also guarantees the SPR properties of $\{(A + \mu I + \frac{1}{\mu^*}B\Psi - L_\rho C), B, S_1 C\}$ for $\forall\Psi$ that $\|\Psi\| \leq \Psi^*_{max}$ and $\forall\mu$ that $0 \leq \mu \leq \mu^*$.

Since $\{(A + \mu I - LC), B, S_1 C\}$ is SPR by design (see Lemma 6), Eq.(74) and Eq.(19) holds for a $P > 0$ and $\bar{Q}$ in (35). Therefore, the following equation also holds:

$$\begin{aligned}(A + \mu I + \frac{1}{\mu^*}B\Psi - LC)^T P + P(A + \mu I + \frac{1}{\mu^*}B\Psi - LC) &\leq -\widetilde{Q} + \frac{1}{\mu^*}PB\Psi^T + \frac{1}{\mu^*}\Psi B^T P \\ &= -\widetilde{Q} + \frac{1}{\mu^*}CS_1\Psi^T + \frac{1}{\mu^*}\Psi S_1^T C^T \end{aligned} \tag{82}$$

where $\widetilde{Q} = \bar{Q} + \bar{C}R^{-1}\bar{C} > 0$. Because of the extra $CS_1\Psi^T$ term, the right hand side of (82) may not be negative definite. Adding an extra term $2\rho C^T S^T S C$ on both sides of Eq.(82) yields

$$\begin{aligned}&(A + \mu I + \tfrac{1}{\mu^*}B\Psi - L_\rho C)^T P + P(A + \mu I + \tfrac{1}{\mu^*}B\Psi - L_\rho C) \\ &\qquad \leq -\widetilde{Q} + \frac{1}{\mu^*}CS_1\Psi^T + \frac{1}{\mu^*}\Psi S_1^T C^T - 2\rho C^T S^T S C \triangleq Q_\rho \end{aligned} \tag{83}$$

with L_ρ defined in Eq.(33). We will show that the ρ chosen in (34) will always produce a negative definite Q_ρ. Consider the following block matrix

$$M(\rho) = \begin{bmatrix} -2\rho S^T S & \frac{1}{\mu^*}S_1^T\Psi^T \\ \frac{1}{\mu^*}\Psi S_1 & -\widetilde{Q} \end{bmatrix}. \tag{84}$$

$\widetilde{Q} < 0$ since Lemma 6 holds for the L and S_1. Using Schur complement, it can be proved that when ρ is picked using inequality (34), $M(\rho) < 0$ for any Ψ bounded by $\|\Psi\| \leq \Psi^*_{max}$. Perform a transformation on $M(\rho)$ using a tall matrix T_C

$$T_C = \begin{bmatrix} C \\ I_{n\times n} \end{bmatrix} \tag{85}$$

shows that

$$Q_\rho = T_C^T M(\rho) T_C = \begin{bmatrix} C^T & I \end{bmatrix}\begin{bmatrix} -2\rho S^T S & \frac{1}{\mu^*}S_1^T\Psi^T \\ \frac{1}{\mu^*}\Psi S_1 & -\widetilde{Q} \end{bmatrix}\begin{bmatrix} C \\ I \end{bmatrix} < 0. \tag{86}$$

The last inequality holds because $M(\rho) < 0$ and T_C does not have a right null space. Combining Eq.(83)(86) and (19) proves that $\{(A + \mu I + \frac{1}{\mu^*}B\Psi - L_\rho C), B, S_1 C\}$ is SPR. Finally, it is noted that Eq.(21) ensures the boundedness of S and S_1. Ψ^*_{max} in (32) is finite. μ^* is non-zero. As a result, a finite ρ^* always exists, so does a finite L_ρ. □

Proof of Theorem 1

Proof. Choosing $\mu = \mu^*$ and $\Psi = \Psi^*$ in Lemma 8 proves that the L_ρ (33) and S_1 (21) guarantees the SPR properties of $\{(A + \mu^* I + \frac{1}{\mu^*} B\Psi^* - L_\rho C), B, S_1 C\}$. Therefore, the results of Lemma 7 holds: i) all signals in the system, including $\widetilde{\Lambda}^T(t) = \Lambda^{-1}(t) - \Lambda^{*-1}$ and $\widetilde{\Theta}^T(t) = \Theta^T(t) - \Theta^{*T}$, are bounded and; ii) state error $e_x(t) \to 0$ as $t \to \infty$, which implies $e_y(t) \to 0$ as $t \to \infty$.

To prove iii), similar to $e_{pz}(t) = z(t) - z_{cmd}$, denote $e_{mz}(t) = z_m(t) - z_{cmd} + L_e C e_x$ where L_e is the corresponding rows of L_ρ. $\int e_{pz}(t)dt$ is a state of x and $\int e_{mz}(t)dt$ is a state of x_m (see Section 1). As a result, the fact $e_x(t) \to 0$ as $t \to \infty$ implies that

$$\left[\int e_{pz}(t)dt - \int e_{mz}(t)dt\right] \to 0, \quad as\ t \to \infty. \tag{87}$$

Substituting the definitions of $e_{pz}(t)$ and $e_{mz}(t)$ transforms (87) into

$$\left\{\int [z(t) - z_{cmd}]dt - \int [z_m(t) - z_{cmd} + L_e C e_x]dt\right\} \to 0, \quad as\ t \to \infty. \tag{88}$$

Since z_{cmd} is piecewise continuous and both $z(t)$ and $z_m(t)$ are integrable, Eq.(88) can be simplified as

$$\int e_z(t)dt \to L_e C \int e_x dt < \infty, \quad as\ t \to \infty. \tag{89}$$

where $e_z(t) = z - z_m$. On the other hand, using the definition of z in (10) and definition of z_m in (13), $e_z(t)$ has the following expression

$$e_z = C_z e_x + D_z \Lambda^* \Theta^{*T} [\Phi(x_p) - \Phi(x_{mp})] + D_z \Lambda^* [\widetilde{\Lambda}^T u_{bl} - \widetilde{\Theta}^T \Phi(x_{mp})] \tag{90}$$

whose derivative is

$$\dot{e}_z = C_z \dot{e}_x + D_z \Lambda^* \Theta^{*T} [\Phi_{x_p} \dot{x}_p - \Phi_{x_{mp}} \dot{x}_{mp}] + D_z \Lambda^* [\dot{\widetilde{\Lambda}}^T u_{bl} + \widetilde{\Lambda}^T \dot{u}_{bl} - \dot{\widetilde{\Theta}}^T \Phi - \widetilde{\Theta}^T \Phi_{x_{mp}} \dot{x}_{mp}] \tag{91}$$

where $\Phi_{(\cdot)}$ stands for $\frac{\partial \Phi}{\partial (\cdot)}$. Because all signals in the system are bounded and Φ is globally differentiable, $\dot{e}_z$ is bounded. Applying Barbalat's Lemma shows that $e_z(t) \to 0$ as $t \to \infty$, which proves iii). □

Proof of Lemma 9

Proof. Define $\phi_p(s) = (sI - A_p)^{-1}$, $\phi(s) = (sI - A)^{-1}$, $\overline{\phi}(s) = (sI - A + BK)^{-1}$ and $\overline{\phi}_L(s) = (sI - A + BK + L_\rho C)^{-1}$. Denote $\bar{R}^{-1} = R^{-1} + \rho I$. As $\epsilon \to \infty$ or $\rho \to \infty$, $\bar{R}^{-1} \to \infty$ and

$$L_\rho = \bar{B}\bar{R}^{-1} S \to \infty. \tag{92}$$

For loop gain at input, we can treat the error integrator (introduced in Section 1) as a part of the plant. The loop gain at input for a LQR controller is

$$L_u^*(s) = K\phi B \tag{93}$$

The loop gain at input for a observer-based controller with a L_ρ and the same K is

$$L_u(s) = K[sI - A + BK + L_\rho C]^{-1} L_\rho C \phi B \tag{94}$$

To prove i), define $\bar{K} \in \mathbb{R}^{p \times n}$ as

$$\bar{K} = \begin{bmatrix} K \\ 0_{(p-m)\times n} \end{bmatrix} \tag{95}$$

such that $BK = \bar{B}\bar{K}$. The asymptotic relation (92) implies

$$\begin{aligned} \bar{L}_u(s) &\triangleq \bar{K}[sI - A + BK + L_\rho C]^{-1} L_\rho \phi \bar{B} && (96)\\ &= \bar{K}[sI - A + \bar{B}\bar{K} + L_\rho C]^{-1} L_\rho \phi \bar{B} && (97)\\ &\to \bar{K}\phi\bar{B}. && (98) \end{aligned}$$

Given (97), the proof of (98) can be found in Ref.[9], which can be applied here because $C\phi\bar{B}$ is square and minimum phase. The partition (95) and (20) shows that element-wise convergence holds, i.e. the submatrix L_u

$$L_u(s) \triangleq K[sI - A + BK + L_\rho C]^{-1} L_\rho C\phi B \to K\phi B \tag{99}$$

as $\epsilon \to \infty$ or $\rho \to \infty$, which proves i).

For loop gain at output, we have to include the error integrator in our controller. Divide $K = [K_p, K_i]$ where $K_p \in \mathbb{R}^{m\times n_p}$ and $K_i \in \mathbb{R}^{m\times r}$. For a LQR controller, the loop gain at output is

$$L_o^*(s) = \left(\begin{bmatrix} I_{n_p} \\ C_{pz} \end{bmatrix} \phi_p(s) B_p + \begin{bmatrix} 0 \\ D_{pz} \end{bmatrix} \right) \begin{bmatrix} K_p & \frac{1}{s} K_i \end{bmatrix} \tag{100}$$

Divide $L_\rho = [L_p, L_i]$ where $L_p \in \mathbb{R}^{n\times p_p}$ and $L_i \in \mathbb{R}^{n\times r}$. Define

$$A_k = \begin{bmatrix} A - BK - L_\rho & L_i \\ 0 & 0 \end{bmatrix}; \quad B_k = \begin{bmatrix} L_p & 0 \\ 0 & I \end{bmatrix}; \quad C_k = \begin{bmatrix} K & 0 \end{bmatrix} \tag{101}$$

For the LQG controller, the transfer function of the controller is $C_k(sI - A_k)^{-1}B_k$ and the loop gain at output is

$$\begin{aligned} L_o(s) &= \left(\begin{bmatrix} C_p \\ C_{pz} \end{bmatrix} \phi_p(s) B_p + \begin{bmatrix} 0 \\ D_{pz} \end{bmatrix} \right) C_k(sI - A_k)^{-1} B_k & (102) \\ &= \left(\begin{bmatrix} C_p \\ C_{pz} \end{bmatrix} \phi_p(s) B_p + \begin{bmatrix} 0 \\ D_{pz} \end{bmatrix} \right) K\bar{\phi}_L(s) \begin{bmatrix} L_p & \frac{1}{s} L_i \end{bmatrix}. & (103) \end{aligned}$$

From (102) to (103), we used the identity

$$(sI - A_k)^{-1} = \begin{bmatrix} \bar{\phi}_L & \bar{\phi}_L L_i \frac{1}{s} \\ 0 & \frac{1}{s} \end{bmatrix}.$$

To prove ii), we need to rely on an asymptotic relation

$$\begin{aligned} \bar{\phi}_L L_\rho &= [\bar{\phi}^{-1} + L_\rho C]^{-1} L_\rho & (104) \\ &= \bar{\phi}[I + L_\rho C\bar{\phi}]^{-1} L_\rho & (105) \\ &= \phi[I + BK\phi + L_\rho C\phi]^{-1} L_\rho & (106) \\ &= \phi \left\{ I + \bar{B}[\bar{K} + \bar{R}^{-1} S C]\phi \right\}^{-1} \bar{B}\bar{R}^{-1} S & (107) \\ &= \phi\bar{B} \left\{ I + [\bar{K} + \bar{R}^{-1} S C]\phi\bar{B} \right\}^{-1} \bar{R}^{-1} S & (108) \\ &\to \phi\bar{B}[C\phi\bar{B}]^{-1} & (109) \end{aligned}$$

as $\epsilon \to \infty$ or $\rho \to \infty$. From (105) to (109), we used the equality $\bar{\phi} = \phi[I + BK\phi]^{-1}$, the design L_ρ, the equality $BK = \bar{B}\bar{K}$, the matrix equality $X[I + XY]^{-1} = [I + YX]^{-1}X$, and the asymptotic relation (92). It is noted that $[C\phi(s)\bar{B}]$ is invertible except at its transmission zeros, and therefore is invertible for all s on the imaginary axis, which is the region of our frequency domain analysis. Now we proceed to prove ii). Since $\phi\bar{B}[C\phi\bar{B}]^{-1}$ is a right inverse of C, we can write

$$C^\dagger(s, \bar{B}) := \phi\bar{B}[C\phi\bar{B}]^{-1} = \begin{bmatrix} C_p^\dagger(s, \bar{B}) & \frac{1}{s} M_p(s, \bar{B}) \\ 0 & I_r \end{bmatrix} \tag{110}$$

where $C_p^\dagger(s, \bar{B})$ satisfies $C_p C_p^\dagger(s, \bar{B}) = I_{p_p}$. and $M_p(s, \bar{B}) \in \mathbb{R}^{p_p\times r}$ satisfies $C_p M_p(s, \bar{B}) = 0_{p_p\times r}$. Since $0 < |s| < \infty$, when $L_\rho \to \infty$

$$K\bar{\phi}_L(s) \begin{bmatrix} L_p & \frac{1}{s} L_i \end{bmatrix} \to \begin{bmatrix} K_p & \frac{1}{s} K_i \end{bmatrix} C^\dagger(s, \bar{B}). \tag{111}$$

Combining (103) and (111) yields

$$\begin{aligned} L_o(s) &\to \left(\begin{bmatrix} C_p \\ C_{pz} \end{bmatrix} \phi_p(s) B_p + \begin{bmatrix} 0 \\ D_{pz} \end{bmatrix} \right) \begin{bmatrix} K_p & \frac{1}{s} K_i \end{bmatrix} C^\dagger(s, \bar{B}) & (112) \\ &= C \left[L_o^*(s) \right] C^\dagger(s, \bar{B}) & (113) \end{aligned}$$

as $\epsilon \to \infty$ or $\rho \to \infty$, which proves ii). □